Title
Patient-derived models of IDH1-mutant, hypermutated glioma

Author
Jones, Lindsey Elise

Publication Date
2018

Peer reviewed|Thesis/dissertation

Patient-derived models of IDH1-mutant, hypermutated glioma

by

Lindsey Elise Jones

DISSERTATION

Submitted in partial satisfaction of the requirements for the degree of

DOCTOR OF PHILOSOPHY

in

Biomedical Sciences

in the

GRADUATE DIVISION

of the

UNIVERSITY OF CALIFORNIA, SAN FRANCISCO

Approved:

[redacted]

Committee in Charge

To my parents, Curt and Sarah, and my partner, Thomas

For your constant support and encouragement

Acknowledgements

I would like to thank my mentor, Dr. Joseph Costello, for providing a positive training environment, giving scientific guidance, encouraging well-being, and supporting novel career exploration during my graduate work. I am grateful for the collaborative, collegial environment that he has fostered in our group. I would like to thank my thesis committee, Dr. Joanna Phillips, Dr. Russ Pieper, and Dr. Aaron Tward for providing feedback on my experiments and progress.

I am very grateful to the faculty of the Nebraska Wesleyan University Biology Department, particularly Dr. Jerry Bricker, and Dr. Garry Duncan, for nurturing my love of science and encouraging me to pursue scientific research and a PhD. Without your guidance, push, and opportunities to hone my craft, I would not be where I am today.

UCSF, in particular the Biomedical Sciences graduate program, has been a wonderful place to call home for the last five years. My work could not have been achieved without advice and assistance from many faculty, students, and staff.

I would like to acknowledge the Brain Tumor Center Tissue Core for their work in identifying patients of interest and receiving fresh and frozen surgical specimens. I would also like to thank the UCSF Department of Neurological Surgery for collecting the surgical specimens.

To my partner, Thomas Hennings: Thank you for being an amazing, intelligent, and supportive partner through the late nights, crazy experiments, and ups and downs of graduate school. I could not have done this without you.

Finally, I would like to thank my parents, Curt and Sarah Jones. I am grateful for their encouragement to pursue my interests, curiosity and desire to learn more about my work, and never-ending reiteration that I can do anything I set my mind to.

Patient-derived models of *IDH1*-mutant, hypermutated glioma

Lindsey Elise Jones

ABSTRACT

Gliomas are a group of central nervous system tumors that are classified based upon histopathological and molecular features. IDH-mutant low-grade gliomas (LGG) are prognostically favorable tumors and are often treated with temozolomide, but can undergo malignant progression via TMZ-induced hypermutation. Cell cultures that faithfully model this genetically distinct and clinically relevant hypermutated (HM) tumor subgroup are lacking, and are necessary to advance our understanding of HM tumors. We established patient-derived cell culture and xenograft models of HM oligodendroglioma and astrocytoma that faithfully recapitulate the molecular and functional features observed in their tumor of origin. We thoroughly characterized these cell lines and established that they are suitable for studying HM glioma, IDH-driven phenotypes, *TERT* promoter- and alternative lengthening of telomeres-driven cellular immortality, therapy-driven evolution, and intratumoral heterogeneity. These models have been widely shared with the neuro-oncology community and accelerated research at institutions across the United States.

TABLE OF CONTENTS

LIST OF TABLES

LIST OF FIGURES

CHAPTER 1: INTRODUCTION

1.1 GLIOMA AND ITS CLASSIFICATION

Gliomas comprise about 30% of central nervous system tumors, originate from glial cells, and occur in the brain or spinal cord. Gliomas are further classified based upon histological features that they share with normal glial cells (astrocytes, oligodendrocytes, and ependymal cells), and include astrocytoma, oligodendroglioma, or ependymoma. Traditionally, glioma subtypes were determined only by histopathological analysis, but revised World Health Organization (WHO) guidelines in 2016 incorporated the use of molecular markers (*1*). Gliomas are further stratified, or graded, by histopathological evaluation for cellularity, mitotic activity, nuclear pleomorphism, microvascular proliferation, and necrosis. They are graded I to IV, with increasing grade being associated with a greater number of aggressive features. Molecular subtype and grade are often associated with patient survival, treatment response, and malignant potential (*2*).

1.1.i Diffuse oligodendroglioma and astrocytoma

Low-grade (WHO grade II), or diffuse oligodendroglioma and astrocytomas are slow growing, infiltrative tumors that typically occur in the cerebrum, and often in the frontal lobe, of adults (*3, 4*). Histologically, they are characterized by nuclear atypia of oligodendrocyte-like or astrocyte-like cells. Molecularly, they are characterized by point mutations in isocitrate dehydrogenase 1 (*IDH1*) or isocitrate dehydrogenase 2 (*IDH2*) (*5*). 80-90% of LGG harbor a heterozygous point mutation in *IDH1* that yields an amino acid change at the 132nd position from an arginine to a histidine (R132H), while 10-20% will harbor other *IDH1* or *IDH2* mutation (*6*). IDH-mutant tumors have a significantly better prognosis than IDH-wt tumors (*7-9*).

Diffuse oligodendroglioma is molecularly characterized by 1p and 19q chromosomal arm co-deletions (1p/19q codel), which likely occurs as a single translocation event (*10, 11*). Studies to identify potential tumor suppressor genes on these chromosomal regions have found mutations in capicua transcriptional repressor (*CIC*) and far upstream element binding

protein 1 (*FUBP1*), which are located on 19q and 1p, respectively (*5, 12, 13*). But, they are only mutated in about 50-70% and 15-30% of oligodendrogliomas, respectively, and their role(s) in gliomagenesis and/or tumor maintenance are not yet clear. These tumors often present with mutation of the telomerase reverse transcriptase (*TERT*) promoter (*TERTp*-mutant), which increases *TERT* expression and allows tumor cells to escape replicative senescence (*8, 14*).

Diffuse astrocytoma is molecularly characterized as 1p/19q intact. It often harbors loss of alpha-thalassemia/mental retardation, X-linked (*ATRX*) (*15*), which is associated with the alternative lengthening of telomeres (ALT) phenotype, and allows for cellular immortality (*16*). Mutation of tumor protein 53 (*TP53*), a well-established tumor suppressor gene, occurs in 94% of WHO grade II astrocytomas that have *IDH* and *ATRX* mutations (*17, 18*).

1.1.ii Anaplastic astrocytoma and oligodendroglioma, glioblastoma

Anaplastic (WHO grade III) oligodendroglioma and astrocytoma share the molecular alterations of WHO grade II glioma, but histologically demonstrate increased mitotic activity. About 4500 patients are diagnosed with grade II or grade III oligodendroglioma or astrocytoma annually (*19*), which we collectively refer to as lower-grade glioma (LGG). Despite clinical intervention, which is discussed below, glioma is a disease that recurs. The time to recurrence is highly variable, and some LGG can recur as a low-grade tumor, while others undergo malignant progression and recur as a higher-grade tumor (*20*). The frequency of malignant progression is variable, and has been reported to range from 17-73% (*21*). Malignant progression is associated with activation of MYC and RTK-RAS-PI3K pathways (*22*) and marked by activation of cell cycle and proliferation (*23*).

High-grade glioma, or WHO grade IV astrocytoma, consists of two distinct disease entities. WHO grade IV IDH-mutant glioblastoma (GBM), or secondary GBM, is an aggressive tumor that evolves from grade II or grade III astrocytoma. Primary GBM, also WHO grade IV, is

a distinct tumor entity, is typically IDH wt, has unique molecular alterations, is fast-growing, and is associated with poor survival (*24*).

1.2 ISOCITRATE DEHYDROGENASE

Mutation of *IDH1* or *IDH2* is a key molecular alteration in LGG; it is the earliest known event in gliomagenesis (*7, 25, 26*). IDH mutation was first identified in primary GBM, but now defines LGG. IDH mutations are missense point mutations, heterozygous, and the majority occur at IDH1 R132H (*25*). Mutant IDH1 R132H can be identified with immunohistochemical (IHC) staining of surgical specimens. Suspected LGG that are negative for IDH1 R132H IHC should have sequencing of IDH1 codon 132 and IDH2 codon 172 performed, as IDH status is important for clinical stratification.

Normal IDH1 or IDH2 protein forms a homodimer and functions to convert isocitrate to α-ketoglutarate. In cancers like glioma and leukemia, mutant IDH1 or IDH2 will form a heterodimer with its wt counterpart, where it will still convert isocitrate to α-ketoglutarate, but subsequently converts α-ketoglutarate to 2-hydroxyglutarate (2-HG) (*27, 28*). 2-HG is a competitive inhibitor of α-ketoglutarate-dependent dioxygenases (*29*), which includes the TET family of enzymes that are important in DNA demethylation (*30*). Inhibition of demethylation leads to epigenetic disregulation (*31*), which in IDH-mutant glioma leads to a CpG island methylator phenotype, or G-CIMP (*32, 33*). G-CIMP gliomas have greater progression-free and overall survival than their IDH wt counterparts (*34-37*). In addition to increased DNA methylation, 2-HG impairs histone demethylation in glioma, which can block cellular differentiation (*38*), and dysregulate insulators, leading to oncogene activation (*39*).

Since IDH mutation is the earliest event in gliomagenesis, it is an attractive therapeutic target. Mutant IDH inhibitors have been developed that block 2-HG production and delay growth of glioma cells *in vitro* (*40*). 2-HG induces a homologous recombination defect that yields cells sensitive to PARP inhibitors, suggesting that the FDA-approved PARP inhibitor

olaparib may have clinical utility in glioma (*41*). Additionally, 2-HG inhibits ALKBH-mediated DNA repair, which sensitizes cells to alkylating agents (*42*).

1.3 TREATMENT OF LOWER-GRADE GLIOMA

1.3.i Surgery

The first line of treatment for LGG is often surgery, which aims to increase survival, improve quality of life, and obtain tissue for diagnosis. Randomized trials evaluating benefits of extensive surgery are lacking, but total or near-total resection is associated with better outcomes (*43-47*). Intraoperative functional mapping (*48*) and imaging techniques like intraoperative MRI (*49, 50*) and aminolevulinic acid (5-ALA) fluorescence-guided surgery (*51*) can help achieve safe total or near-total resections. Surgery is frequently followed by chemotherapy (*52*), or for patients who are “high risk” (age greater than 40, subtotal resection or biopsy only), chemoradiotherapy (*53, 54*).

1.3.ii Chemotherapy

PCV (procarbazine, lomustine (CCNU), and vincristine) and temozolomide (TMZ) are often used to treat LGG, despite that most of the evidence for their clinical utility has come from studies in anaplastic tumors, recurrent tumors, or primary GBM. PCV has been proven effective in anaplastic oligodendrogliomas (*55, 56*). The benefit of TMZ was first shown to improve survival in GBM conjunction with radiotherapy (*57*), and has recently been reported to have a survival benefit in newly diagnosed anaplastic astrocytoma (*58*). TMZ is well-tolerated by patients (*54, 59*), and therefore has been adopted to treat primary LGG. 1p/19q co-deleted oligodendrogliomas in particular see pronounced survival benefit with chemotherapy treatment (*56, 60*).

1.3.iii Radiotherapy

The administration of radiotherapy is associated with an increase in progression-free survival (PFS) (*61*). Although the ideal dose of radiotherapy has not yet been established for LGG, 50.4 Gy are typically given in fractions of 1.8 Gy, with fewer side effects observed at lower dosage (*62, 63*). The potential long overall survival (OS) of LGG patients raises concerns about possible radiation-associated cognitive defects.

1.4 TEMOZOLOMIDE-INDUCED HYPERMUTATION

1.4.i Mechanism of cytotoxicity

TMZ introduces methyl adducts onto guanine (G), and methylation at the O^6 position (O^6-meG) is the adduct most associated with cytotoxicity (*64, 65*). The suicide protein methyl guanine methyl transferase (*MGMT*) can directly remove O^6-meG, but is degraded in the process. Methylation of the *MGMT* promoter, which leads to decreased *MGMT* expression (*66, 67*) and subsequent persistence of O^6-meG adducts, is associated with increased OS of GBM patients treated with chemoradiotherapy with alkylating agents like TMZ (*68-70*). O^6-meG causes a mispairing of guanine with thymine (T), which is recognized by the DNA mismatch repair (MMR) machinery. The MMR system repairs the T, but leaves behind the O^6-meG lesions, which allows the O^6-meG to mispair with T again. This causes futile cycling of MMR, double-strand DNA breaks, and ultimately, cytotoxicity (*71, 72*).

1.4.ii Loss of mismatch repair

Loss of MMR is known to contribute to chemoresistance in many cancer types, including hereditary nonpolyposis colon cancer (*73*) and GBM (*74, 75*), and has been reported to confer chemoresistance in cancer cell lines (*76, 77*). MMR deficiency can arise from somatic tumor mutations (*78*) and during treatment with alkylating therapy like TMZ (*79, 80*). MMR deficiency is associated with a mutator phenotype (*81-83*). In TMZ treatment, loss of MMR

leads to loss of cytotoxicity (*73*) and accumulation of G:C>A:T nucleotide transitions in the genome (*84*).

1.4.iii A signature of temozolomide-induced hypermutation

A hypermutator signature of G:C>A:T nucleotide transitions has been reported before in TMZ-treated GBM and cells (*80, 85-88*). We and others (*7, 89, 90*) have shown that treatment of LGG with TMZ can lead to TMZ-induced mutations in MMR genes, MMR deficiency, and subsequent TMZ-induced hypermutation. TMZ-induced hypermutation is accompanied by increased MGMT promoter methylation (79), mutations in phosphoinositide 3-kinase (*PI3K*) and protein kinase B (*AKT*) and retinoblastoma (*RB*) pathway genes, and malignant progression to a higher-grade tumor. Hypermutated (HM) tumors represent a unique clinical entity that currently lacks a standard of care. Understanding the evolution of TMZ-induced hypermutation and identifying therapies for patients with HM tumors is a key next step, for which experimental models of LGG are needed.

1.5 EXPERIMENTAL MODELING OF LOWER-GRADE GLIOMA

1.5.i Engineered cell models

Normal human astrocytes have been modified to express E6 and E7 viral oncoproteins (NHA/E6/E7), which inactivate p53 and pRB, respectively (*91, 92*), and will form intracranial tumors when hTERT is overexpressed (NHA/E6/E7/hTERT) (*93*). Overexpression of IDH1 R132H in the NHA/E6/E7 model yields 2-HG production (*94*) and an anaplastic astrocytoma-like model (*95*), which currently serves as one of the best engineered cell models of LGG. However, these cells lack *ATRX* mutation, a key diagnostic molecular feature of diffuse and anaplastic astrocytoma. Additionally, overexpression of mutant IDH1 in NHA/E6/E7IDH1 R132H cells does not model the 1:1 ratio of mutant IDH1 to wt IDH1 in most glioma patients.

We have shown that allelic imbalance of mutant and wt IDH1 can lead to epigenetic reprograming in glioma patients (*96*).

1.5.ii Mouse models

Murine models of LGG are limited and often do not involve key diagnostic molecular alterations or driver mutations. Chemical methods to induce glioma have yielded GBM-like glioma through transplacental delivery of ethyl-nitrosourea in *p53*-null mice (*97*). Similarly, intracranial injection of 3-methylcholantrene yields a GBM-like glioma, which has produced the derivative mouse glioma model GI26 (*98*). While glial fibrillary acidic protein (*GFAP*)-controlled expression of *v-src* kinase in mice can produce early lesions that appear low-grade astrocytoma-like, later tumors histologically mimic GBM (*99*). Overexpression of epidermal growth factor receptor (*EGFR*) by S100 control of *v-erbB*, which transforms EGFR, was found to yield oligodendroglioma-like tumors (*100*), but this model lacks key IDH and *TERT*p mutations. Interestingly, transgenic expression of mutant IDH causes death in mice shortly after birth (*101*), but will form tumors when virally delivered to mice with a genetic background lacking cyclin dependent kinase inhibitor 2A (*Cdkn2a*), phosphate and tensin homolog (Pten), and Atrx (*102*). Additionally, no cases of sporadic, IDH-mutant murine glioma have been reported (*103*). Therefore, no genetic models of murine glioma currently capture the key molecular alterations of human LGG.

1.5.iii Patient-derived lines and patient-derived xenografts

Subsequently, patient-derived cell lines (PDLs) and patient-derived xenograft (PDX) models can be used to better model the molecular alterations and expression patterns seen in human tumors (*104*). The first successful brain tumor PDLs were established as neurospheres, a culturing system that was originally established to culture primary neural stem cells (*105, 106*). Glioma neural stem cell cultures, or GNS cultures, utilize serum-free culture conditions and can be grown either in suspension or adherently. Adherent cultures are experimentally

more tractable than their suspension culture counterparts, and have been shown to be equivalent in their retention of parental tumor features (*107*). PDLs can also be established in serum-containing cultures, but the media in which glioma PDLs are established matters; evidence is growing that PDLs derived in serum-free conditions better model their parental tumors than those derived in serum (*108*).

These PDLs can be injected heterotopically into the flank or orthotopically into the cranium of immunocompromised animals to establish PDXs (*109*). PDXs are ideal for the study of glioma because they retain the key molecular alterations of their parent tumors, like PDLs, but better recapitulate three-dimensional tumor growth, interaction with normal cell types, and can be used for pre-clinical drug screening. They are, however, difficult and timely to establish.

Ideally, IDH-mutant glioma would be studied through PDLs and PDXs, but IDH-mutant PDLs and PDXs have historically been difficult to establish, likely owing to the growth-inhibitory effects of 2-HG. Attempts to derive IDH-mutant PDLs are often accompanied by reports of loss of the mutant or wt allele (*110, 111*), which hampers studies of IDH-associated phenotypes *in vivo*. Similarly, models are needed to study the distinct and clinically-relevant tumor subtype of HM glioma. Some HM glioma PDLs exist, but none have been published that maintain heterozygous IDH mutation and include broad genomic characterization (*5, 112, 113*).

1.6 RESEARCH PURPOSE

In order to better understand TMZ-induced hypermutation in IDH-mutant LGG, we need well-characterized experimental models that faithfully recapitulate the molecular, functional, and evolutionary features of patient tumors. We sought to meet this need through establishing and characterizing PDLs and PDXs from patients originally diagnosed with LGG who were treated with TMZ and were undergoing operation on a recurrent tumor.

CHAPTER 2: PATIENT-DERIVED CELL CULTURES OF *IDH1*-MUTANT, HYPERMUTATED GLIOMA THAT MODEL THE INTRATUMORAL HETEROGENEITY AND FUNCTIONAL FEATURES OF THEIR ORIGINATING TUMORS

2.1 ABSTRACT

IDH-mutant low-grade gliomas (LGG) are prognostically favorable tumors but can undergo malignant progression via temozolomide (TMZ)-treatment associated hypermutation. Patient-derived cell lines (PDLs) that model this genetically distinct and clinically relevant hypermutated (HM) tumor subgroup are lacking. Here, we established and characterized three PDLs and a total of 9 PDL single-cell derived subclones (scPDLs) of post-treatment surgical specimens from two patients originally diagnosed with lower-grade IDH-mutant glioma, including an *ATRX* and *TP53*-mutant HM glioma (astrocytoma), and a *TERT* promoter-mutant, 1p/19q co-deleted HM glioma (oligodendroglioma). We used exome sequencing of the PDLs, parent tumor tissue, xenografts, and blood DNA to elucidate the intratumoral heterogeneity (ITH) and therapy-driven evolution of these models. These models maintained their subtype-defining features over many passages, including retention of the heterozygous IDH1 R132H mutation and sustained production of 2-hydroxyglutarate (2-HG), highlighting their utility for investigating mutant IDH-driven phenotypes. The mutually exclusive mechanisms of telomere maintenance were also retained in the respective PDLs, including a *TERT* promoter mutation in the oligodendroglioma PDL, and *ATRX* mutation and the alternative lengthening of telomeres (ALT) phenotype in the astrocytoma PDLs. The PDLs exhibited the mutational signature of TMZ-induced mutagenesis, and represent the ITH of their originating HM tumors. To further examine the potential of the PDLs for modeling ITH, a critical feature underlying therapeutic failures, scPDL were sequenced, revealing branching evolution within the PDLs. PDLs exhibited anchorage-independent growth in soft agar, highlighting their utility for drug screening. The oligodendroglioma-derived PDL formed infiltrative, intracranial tumors with characteristic oligodendroglioma histology, with a relatively long period to tumor formation, which mirrors tumor behavior in patients. These self-renewing PDLs and scPDLs faithfully represent the genotype and function of the originating HM tumor tissue, while providing new

insight into the unprecedented mutational load and ITH of HM glioma. These PDLs may also serve as models to discover new therapies to prevent, delay, or treat *IDH1*-mutant HM glioma.

2.2 INTRODUCTION

Low-grade (WHO grade II) and anaplastic (WHO grade III) gliomas are relatively slow growing, infiltrative tumors that typically occur in the cerebrum of adults (collectively referred to as lower-grade glioma, or LGG). They are classified as astrocytoma or oligodendroglioma by histology and molecular markers (*1*), with oligodendrogliomas harboring mutation of *IDH1* or *IDH2* (IDH-mutant) and co-deletion of chromosomal 1p and 19q arms (*5*), while astrocytomas harbor IDH mutation, are 1p/19q intact, and often have *ATRX* loss and *TP53* mutation. Typically, LGG are treated with surgical resection followed by chemotherapy (*52*), but patients considered “high risk” with an age greater than 40 or subtotal resection or biopsy only will receive chemoradiotherapy (*53, 54*), most commonly with temozolomide (TMZ). Despite clinical intervention, glioma is a disease that recurs (*21*). The time to recurrence can be highly variable, and some LGG may recur as a low-grade tumor, while others may undergo malignant progression and recur as a higher-grade tumor (*20*).

We and others have shown that TMZ-treated LGG can undergo hypermutation after treatment (*22, 89, 90, 114*). Chemotherapy-associated hypermutation in LGG and HGG is characterized by an increased mutational burden, and is often accompanied by mismatch repair (MMR) deficiency (*80, 83, 86, 87, 115, 116*). Hypermutation in LGG is characterized by mutations in MMR and PI3K-AKT-mTOR signaling genes and is dominated by C:G>A:T nucleotide transitions (*89*). Hypermutation has also been reported in post-treatment primary glioblastoma (GBM) (*87*). Our findings have informed the design of a clinical trial (NCT02023905) to address hypermutation in LGG, which highlights the need for clinical strategies to study hypermutation and post-treatment glioma. Hypermutated (HM) tumors demonstrate intratumoral heterogeneity (ITH), which is a critical feature that underlies

therapeutic failure. Additionally, HM tumors have been shown to be good candidates for successful immunotherapies due to increased candidate neoantigenic targets.

Increasing attention is being drawn to the necessity to thoroughly and longitudinally characterize *in vitro* and *in vivo* cancer models (*117, 118*). At least two HM glioma PDLs have been reported that maintain heterozygous IDH mutation, though without broad genomic characterization. Kelly et al. established a 1p/19q co-deleted cell line, BT-088, that was IDH wildtype (wt) and resistant to chemotherapy (*112*). In 2012, Yip *et al*. performed whole-genome sequencing on BT-088, showing it to be hypermutated (*5*). Wakimoto *et al*. established seven xenografts with heterozygous *IDH1* mutation that maintained 2-HG production through serial xenografting (*113*). Of these seven IDH-mutant xenografts, three were treated with TMZ, and two acquired tertiary mutations, suggesting that they might be HM, but were only evaluated for select oncogenic mutations. Some of these PDLs have been used in additional studies by this group, but have been best metabolically characterized (*119, 120*).

In this study, we provide in-depth genomic and functional characterization of self-renewing PDL and PDX models of *IDH1*-mutant HM glioma, and further elucidate the evolutionary and therapy-driven features of these genetically distinct but poorly characterized and tumors. We established three *IDH1*-mutant, HM glioma PDLs from two post-treatment surgical specimens – two lines (SF10602 GNS and SF10602 FBS) from an *ATRX*- and *TP53*-mutant, HM astrocytoma patient (P137), and one (SF10417 GNS) from a *TERT* promoter (*TERT*p)-mutant, 1p/19q co-deleted, HM oligodendroglioma patient (P278).

2.3 RESULTS

2.3.i Patient characteristics and clinical histories

Tissue for P137 was acquired from the second recurrence of a female originally diagnosed with a grade III astrocytoma. The patient received two rounds of TMZ before this second recurrence – one round after surgical resection of the primary tumor, and one round

after surgical resection of the first recurrence (Fig 2.1a). Tissue for P278 was acquired from the third recurrence of a male patient initially diagnosed with a grade II oligodendroglioma. This patient received two rounds of TMZ before this third recurrence – one round prior to resection of the first recurrence, and one prior to resection of the second recurrence (Fig 2.1d). PDLs were successfully established in GNS and FBS conditions from P137 tissue, while P278 tissue yielded a GNS culture.

2.3.ii Patient-derived cell lines faithfully capture and model hypermutated oligodendroglioma and astrocytoma biology

Exome libraries prepared from P137 and P278 tumor, blood (normal), PDL, scPDL, and xenograft samples all had coverage of greater than 83X (Table 2.1). Exome sequencing revealed all P137 tumor samples had mutations in *IDH1*, *ATRX*, and *TP53*, and all SF10602 samples to be HM. For this patient, SF10602 GNS (SF10602 GNS P4) was found to be a mixture of two subclones, and was split into two groups based on evidence of shared mutations with the culture adjacent (CA, SF10602 CA) or SF10602 FBS (SF10602 FBS P2) samples. The two distinct populations of SF10602 GNS P4, SF10602 GNS P4-1, and SF10602 GNS P4-2, and SF10602 FBS cultures had 2276, 2351, and 2925 mutations, respectively, and phylogenetic analysis revealed that these cell lines represented independent hypermutation events compared to each other and to spatially distinct and adjacent uncultured tissue (Fig 2.1b). Comparison of mutational profiles suggests that a subclone of SF10602 GNS was selected during additional passages in culture and luciferase modification (SF10602 LUC-GNS P17), but was related to other single-cell clones derived from SF10602 GNS P21 (clones 8, 20, 2, 17, and 10). The first recurrence of P137, SF10071, which was post-TMZ treatment, was not HM, but did demonstrate some intratumoral heterogeneity (Fig 2.1c). An additional *IDH1*-

mutant cell line was derived from the first recurrence of this tumor (SF10071 GNS P9) and subjected to exome sequencing, but was not further characterized.

HM P137 SF10602 samples acquired TMZ-associated C:G>A:T nucleotide transitions in MMR and PI3K pathway genes, supporting previous reports of other TMZ-treated, HM patients. These mutations led to a dominant mutational signature 11 (Fig 2.2a), which is associated with TMZ (*121*), and a sub-signature 6 in the FBS line and parental tumor (SF10602 v1), which is associated with MMR deficiency. HM SF10602 samples also had sub-signature 15, which is also associated with MMR deficiency. P137 SF10071, which was not HM, did not show evidence of signatures 11 or 6. Instead, it had a strong mutational signature 1A, which is associated with patient age and spontaneous deamination of 5-methyl cytosine.

P278's PDL, SF10417 GNS P5, was HM with 5692 mutations. 3967 of these mutations are shared with three spatially distinct pieces of the tumor (SF10417 Cy, SF10417 Y, and SF10417) that were also HM (Fig 2.1e). SF9818 was an independent hypermutation event with 1599 mutations. A subclone was selected through culture time and luciferase modification (SF10417 LUC-GNS P33), but was closely related to single-cell clones derived from SF10417 GNS P22 (clones 24, 36, 8, and 20). SF10417 GNS yielded intracranial tumors in nude mice, and further evolved *in vivo* (SF10417 Xeno). A cell line was derived from this mouse tumor (SF10417 Xeno-GNS P6) and was genetically similar to its tumor of origin. All P278 tumor samples harbored 1p/19q co-deletion and mutations in *IDH1*, *TERT*p, *CIC*, and *FUBP1* (Table S3).

HM SF10417 samples from P278 also acquired TMZ-associated C:G>A:T nucleotide transitions in mismatch repair (MMR) and PI3K pathway genes, and as a result, had a dominant mutational signature 11 and sub-signature 6 (Fig 2.2b). Signature 6 was not seen in all samples, including the independent hypermutation event in Recurrence 2. The HM samples from this patient with the greatest mutational burdens were close to each other on the phylogenetic tree and had sub-signature 1A. TMZ-associated mutational signature data from

both patients show that, despite divergence between some samples, all cell lines we established were clones that captured the mutational processes driving tumor evolution in the patient of origin.

2.3.iii Patient-derived cell lines faithfully model canonical drivers.

Despite the complex evolution of these tumors, their derivative PDLs retained canonical drivers. SF10602 GNS, SF10602 FBS, and SF10417 GNS maintained heterozygous *IDH1* R132H through culture time and produced 2-HG (Fig. 2.3). While 2-HG production dropped over the course of passage time, it was still produced at late passages.

ATRX-mutant SF10602 GNS and SF10602 FBS were positive for C-circle amplification upon the addition of polymerase Φ29 across multiple passages, while *ATRX*-intact SF10417 GNS was negative for C-circles (Fig. 2.4a). This is consistent with ATRX loss leading to alternative lengthening of telomeres (ALT). The quantity of C-circles increased in SF10602 PDLs through serial culture (Fig 2.4b). UMUC3, an ALT-negative human bladder transitional cell carcinoma cell line, did not show C-circle amplification. U2OS, an ALT-positive human osteosarcoma cell line, demonstrated C-circle amplification. Additionally, SF10602 GNS and SF10602 FBS showed heterogeneous telomere length as measured by telomere restriction fragment analysis (Fig. 2.4c). ALT-negative and *TERT*p-mutant UMUC3 SF10417 GNS had telomeres ranging from ~2-6 kb, consistent with *TERT*p mutations causing maintenance of critically short telomeres, while ALT-positive U2OS, SF10602 GNS, and SF10602 FBS had an accumulation of telomeres at 18.8 kb accompanied by a wide length distribution.

All cell lines demonstrated anchorage-independent growth, which is a key hallmark of transformed cell lines that is not always retained patient-derived cultures (Fig 2.5).

2.3.iv SF10417 GNS forms orthotopic tumors in nude mice

SF10417 luciferase-modified GNS cells orthotopically implanted into nude mice yielded infiltrative tumors in four of nine mice, which recapitulated human oligodendroglioma histology (Fig 2.6 a and b), and maintained IDH1 R132H expression, as measured by IHC on formalin-fixed, paraffin-embedded tissue (Fig 2.6c). A cell line was derived from the tumor shown in Fig 2.6 a-c, and was re-implanted orthotopically into mice. Serial xenografts also formed tumors in three of nine mice that modeled human tumor histological features and expressed IDH1 R132H, but showed a slightly less infiltrative growth pattern (Fig 2.6d-f).

In one serial xenograft case, a change in histology was observed in part of the tumor (Fig 2.6g), with oligodendroglioma histology (left panel) shifting to one with prominent anaplastic features with marked nuclear pleomorphism, macronuclei, and mitotic figures (right panel). This change was accompanied by loss of IDH1 R132H (Fig 2.6h). We have reported on *IDH1* allelic imbalance upon recurrence in human tumors (*96*).

Both *in vivo* passages of luciferase-modified SF10417 GNS formed luminescent tumors, as measured with *in vivo* bioluminescent imaging (Fig 2.6 i and j). The first *in vivo* passage of SF10417 GNS had a very long and variable time-to-endpoint, which mimics the slow progression of LGG in patients. Over the course of serial xenografts, the time-to-endpoint was cut to nearly a third, with three of nine mice presenting with tumors (Fig 2.6k).

2.4 DISCUSSION

Here, we successfully derived and characterized three PDLs that maintain diagnostic molecular features and key oncogenic drivers of astrocytoma and oligodendroglioma. These HM PDLs were derived from recurrent, post-TMZ tumors, and show key genetic alterations associated with HM (*89*), such as high mutation burden, C:G>A:T nucleotide transitions in MMR and PI3K pathway genes, and a TMZ-associated mutational signature. The evidence of mutational signature 11 in the PDLs demonstrates that the differences between samples is a

result of subclonal dynamics and *in vivo* and *in vivo* selection, and that mutations observed in these cell lines originated in the patient. These PDLs and SF10417 xenografts provide opportunities to explore how HM tumors evolve under selective pressure, and to elucidate neoantigens associated with HM that could serve as novel immunotherapy targets.

Similarly, mutation of *IDH1*, particularly at codon 132 in *IDH1*, is likely the earliest genetic event in the development of low-grade glioma (*122*), and IDH1 R132H leads to the production of 2-HG (*123*). We know that 2-HG inhibits α-ketoglutarate-dependent dioxygenases, like TET enzymes (*29*), and leads to a global increase in DNA methylation called G-CIMP (glioma CpG island methylator phenotype) (*32, 33*). But, we still do not fully understand how IDH mutation and 2-HG production contributes to gliomagenesis, tumor maintenance, and/or response to targeted therapies. Our PDLs maintain heterozygous IDH1 R132H through months of *in vitro* culturing, despite many reports of primary glioma lines losing *IDH1* wt or mutant alleles *in vitro* and *in vivo* (*111, 113*), or being unable to grow *in vitro* (*110*), and produce 2-HG. Serial xenografts of SF10417 GNS may provide a way to study allelic imbalance of *IDH* upon recurrence, which has implications for success of targeted therapies.

Additionally, these PDLs provide models in which to study telomerase- and *ALT*-mediated mechanism of cellular immortality, which are relevant to many cancer types and of interest to target therapeutically. These cell lines are invaluable resources to the brain tumor research community, and have already contributed to advancing the work of others (*124-126*).

2.5 TABLES

Table 2.1. Coverage of samples evaluated by exome sequencing.

Sample	Coverage
P278 Normal	98
P278 Recurrence 2	98
P278 Recurrence 3 Y	91
P278 Recurrence 3 Cy	98
P278 Recurrence 3	103
P278 Recurrence 3 GNS P5	102
P278 Recurrence 3 LUC-GNS P33	130
P278 Recurrence 3 Xeno	199
P278 Recurrence 3 Xeno-GNS P6	202
P278 Recurrence 3 GNS Clone 8	97
P278 Recurrence 3 GNS Clone 20	100
P278 Recurrence 3 GNS Clone 24	88
P278 Recurrence 3 GNS Clone 36	84
P137 Normal	91
P137 Recurrence 2 P	111
P137 Recurrence 2 G	83
P137 Recurrence 2 v3	118
P137 Recurrence 2 GNS P9	143
P137 Recurrence 3 v1	117
P137 Recurrence 3 CA	115
P137 Recurrence 3 GNS P4	111
P137 Recurrence 3 FBS P2	98
P137 Recurrence 3 LUC-GNS P17	127
P137 Recurrence 3 GNS Clone 2	90
P137 Recurrence 3 GNS Clone 8	104
P137 Recurrence 3 GNS Clone 10	115
P137 Recurrence 3 GNS Clone 17	113
P137 Recurrence 3 GNS Clone 20	120

2.6 FIGURES

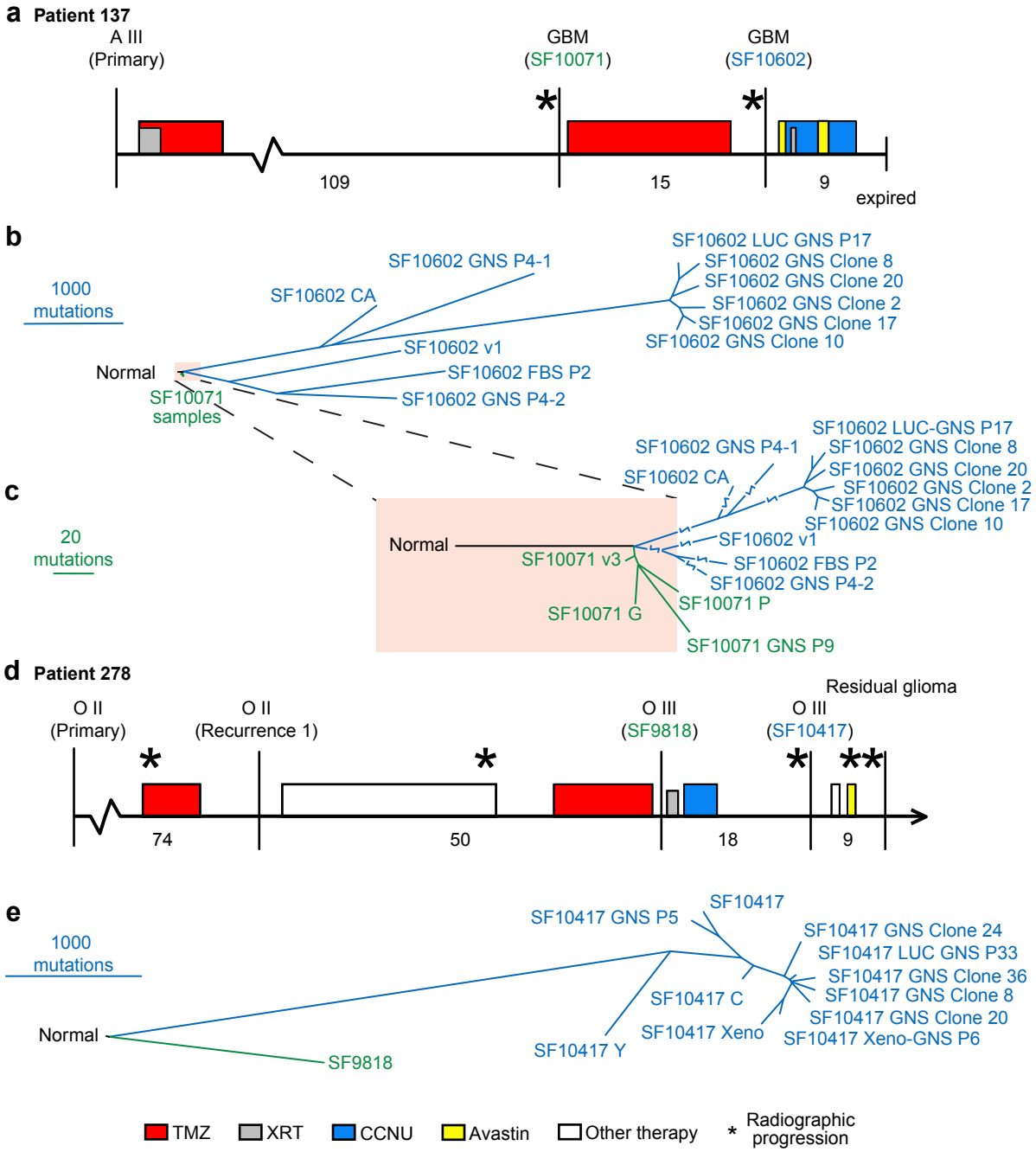

Figure 2.1. Extensive branching evolution and intratumoral heterogeneity of HM clones *in vivo* and *in vitro*.
(a), the timeline and clinical history of Patient 137 (P137) to scale. Vertical lines indicate surgical resection; stars represent radiographic progression; rectangles indicate treatment. Months between surgical resections are given below. Diagnosis according to the 2016 WHO criteria is given above each surgical time point, and surgeries from which samples were sequenced are designated with an SF number. Tumor phylogenies were constructed from single-nucleotide variants calls from exome sequencing data and line length is drawn to scale with mutational burden. **(b)**, fifteen samples were sequenced for P137, including two distinct

hypermutated HM PDLs derived from surgery SF10602; a PDL in GNS medium at passage 4 (SF10602 GNS P4), and a PDL in FBS at passage 2 (SF10602 FBS P2. A luciferase-modified version of the GNS PDL was created and sequenced at passage 17 (SF10602 LUC-GNS P17). Two subclones were identified within SF10602 GNS P4, and are designated as SF10602 GNS P4-1 and SF10602 GNS P4-2. Additionally, single-cell clones were derived from passage 21 of SF10602 GNS, and five were sequenced (SF10602 GNS Clone 8, SF10602 GNS Clone 20, SF10602 GNS Clone 2, SF10602 GNS Clone 17, and SF10602 GNS Clone 10). **(c)**, a zoomed-in view of the relationship between samples of SF10071, which are to scale, compared to the HM samples (not drawn to scale). **(d)**, the clinical history of Patient 278 (P278). Fifteen samples of P278 were sequenced, including one HM PDL in GNS medium at passage 5 (SF10417 GNS P5), and a luciferase-modified version of the GNS PDL at passage 33 (SF10417 LUC-GNS P33). Single-cell clones were derived from passage 22 of SF10417 GNS, and four were sequenced (SF10417 GNS Clone 24, SF10417 GNS Clone 36, SF10417 GNS Clone 8, and SF10417 GNS Clone 20). Additionally, SF10417 GNS formed intracranial tumors in mice, and a sample of xenograft was sequenced (SF10417 Xeno). A piece of this xenograft was used to establish a serial *in vitro* GNS culture, and was sequenced at passage 6 (SF10417 Xeno-GNS P6) **(e)**. *FBS*, media containing 10% fetal bovine serum. *GNS*, glioma neural stem cell. *CA*, culture-adjacent. *C*, *G*, *P*, *Y* surgical specimens that were mapped to tumor imaging. *v1* and *v3*, randomly sampled surgical specimens. *O*, oligodendroglioma; *A*, astrocytoma. *TMZ*, temozolomide. *XRT*, radiation therapy. *CCNU*, lomustine.

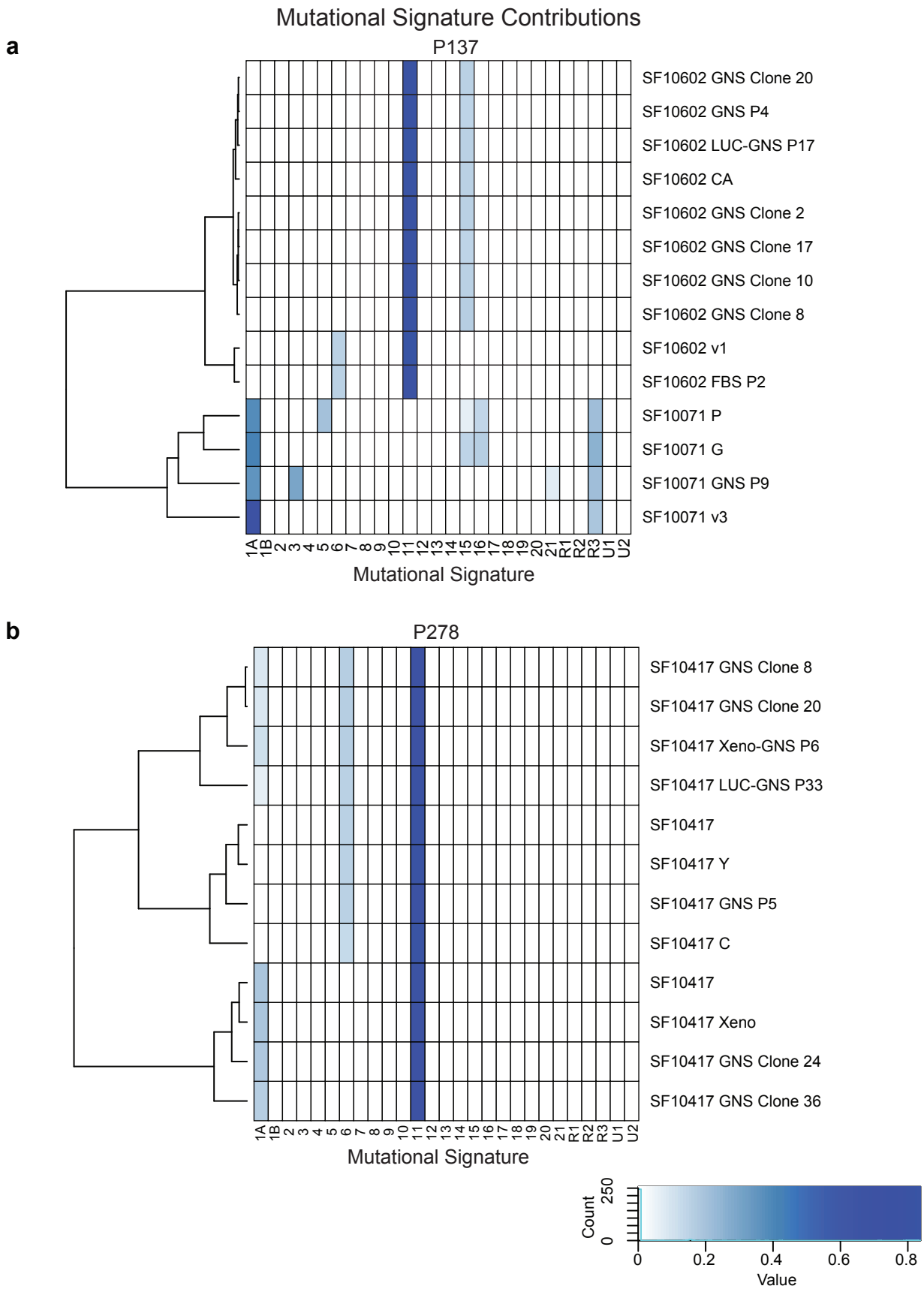
Mutational Signature Contributions
a
P137
SF10602 GNS Clone 20
SF10602 GNS P4
SF10602 LUC-GNS P17
SF10602 CA
SF10602 GNS Clone 2
SF10602 GNS Clone 17
SF10602 GNS Clone 10
SF10602 GNS Clone 8
SF10602 v1
SF10602 FBS P2
SF10071 P
SF10071 G
SF10071 GNS P9
SF10071 v3
1A 1B 2 3 4 5 6 7 8 9 10 11 12 13 14 15 16 17 18 19 20 21 R1 R2 R3 U1 U2
Mutational Signature
b
P278
SF10417 GNS Clone 8
SF10417 GNS Clone 20
SF10417 Xeno-GNS P6
SF10417 LUC-GNS P33
SF10417
SF10417 Y
SF10417 GNS P5
SF10417 C
SF10417
SF10417 Xeno
SF10417 GNS Clone 24
SF10417 GNS Clone 36
1A 1B 2 3 4 5 6 7 8 9 10 11 12 13 14 15 16 17 18 19 20 21 R1 R2 R3 U1 U2
Mutational Signature
Count
0
250
0
0.2
0.4
0.6
0.8
Value

Figure 2.2. HM samples are dominated by mutational signature 11, a signature specifically associated with TMZ treatment (Alexandrov, 2013).
(**a**), exome data from all P137 and (**b**), P278 samples were analyzed for the contribution of known mutational signatures. SF10071 samples are not hypermutated and do not show the TMZ-associated signature, while P137 SF10602 samples are hypermutated and have a strong TMZ-associated signature. All P278 SF9818 and SF10417 samples are hypermutated and have a TMZ-associated mutational signature. Eight SF10417 samples have an increased enrichment of signature 6, which is associated with mismatch repair deficiency. Eight samples also demonstrate an increase in signature 1A which is associated with the endogenous mutational process of cytosine deaminase.

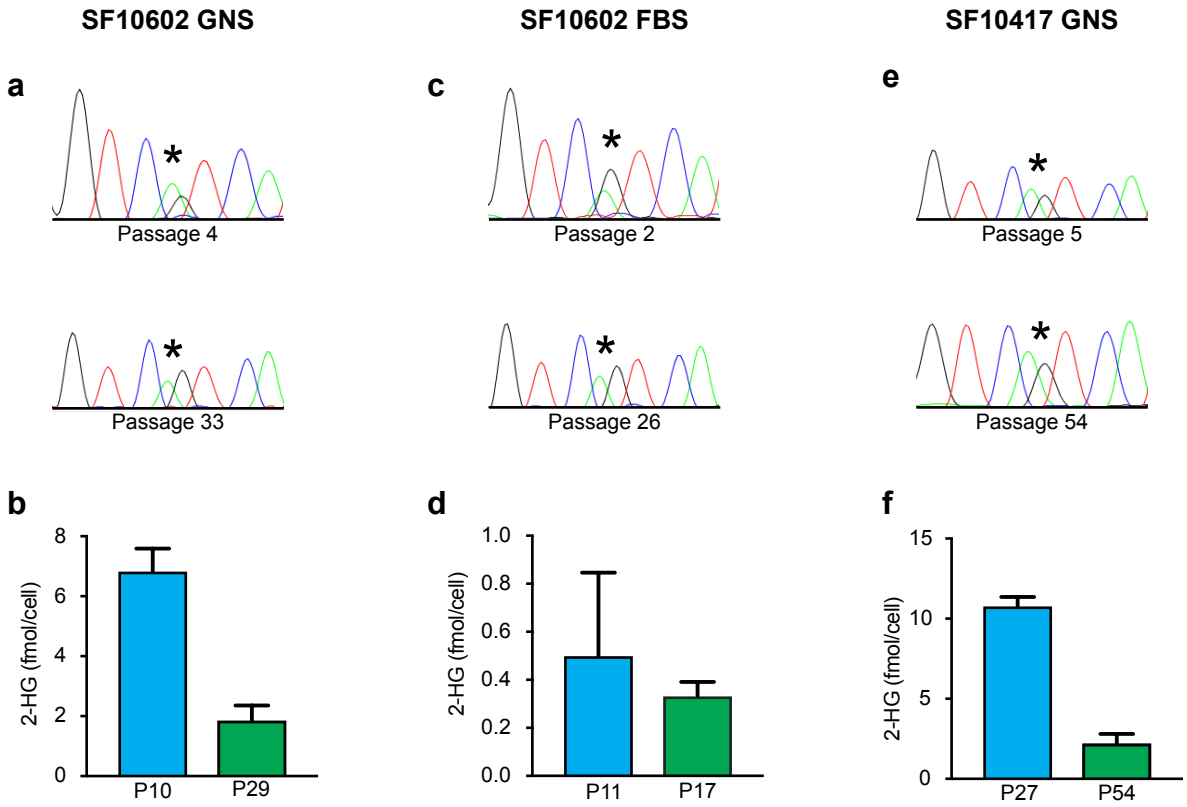

Figure 2.3. HM cell lines retain heterozygous IDH1 R132H through serial passage and continue to produce 2-HG.
(a), SF10602 GNS retains *IDH1* R132H through passage 33, as determined by Sanger sequencing and **(b)**, produces 2-HG, as measured by NMR, through passage 29. **(c)**, SF10602 FBS and maintains *IDH1* R132H through passage 26 and **(d)**, produces 2-HG through passage 17. **(e)**, SF10417 GNS maintains *IDH1* R132H through passage 54 and **(f)**, produces 2-HG through passage 54. * denotes the location of the heterozygous G>A mutation.

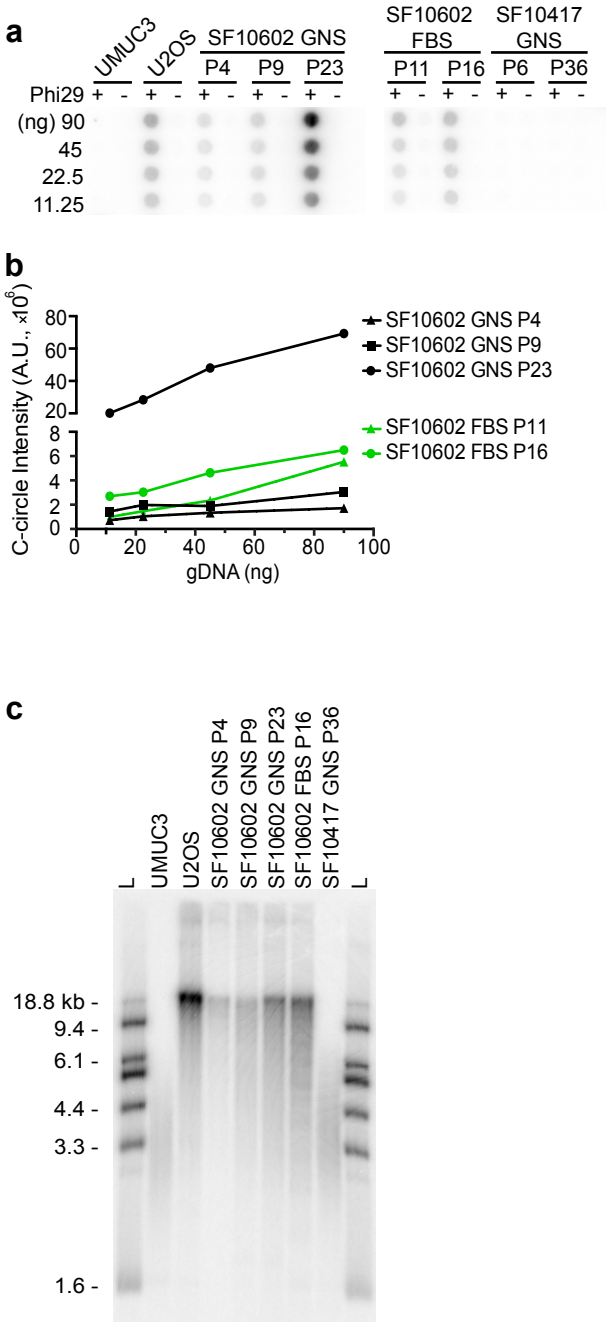

Figure 2.4. *ATRX*-mutant SF10602 GNS and SF10602 FBS are positive for the alternative lengthening of telomeres (ALT) phenotype.
ATRX-mutant SF10602 GNS and SF10602 FBS cultures are positive for C-circle amplification upon the addition of polymerase Phi29 across multiple passages, while *ATRX* wt SF10417 GNS is negative for C-circles. A human bladder transitional cell carcinoma cell line (UMUC3) and a human osteosarcoma cell line (U2OS) serve as negative and positive controls for C-circle amplification, respectively. Signal intensity in (**a**) was (**b**), quantified (in arbitrary units) and plotted. Signal correlates linearly with input DNA, and increases with increasing passage of the PDLs. (**c**), telomere restriction fragment length analysis shows an accumulation of long telomeres in the ALT$^+$ cells, and a heterogeneous telomere length distribution, another

hallmark of ALT. The ALT$^-$ cells (SF10417 GNS P36 and UMUC3) show a tighter and shorter length distribution. *L*, ladder.

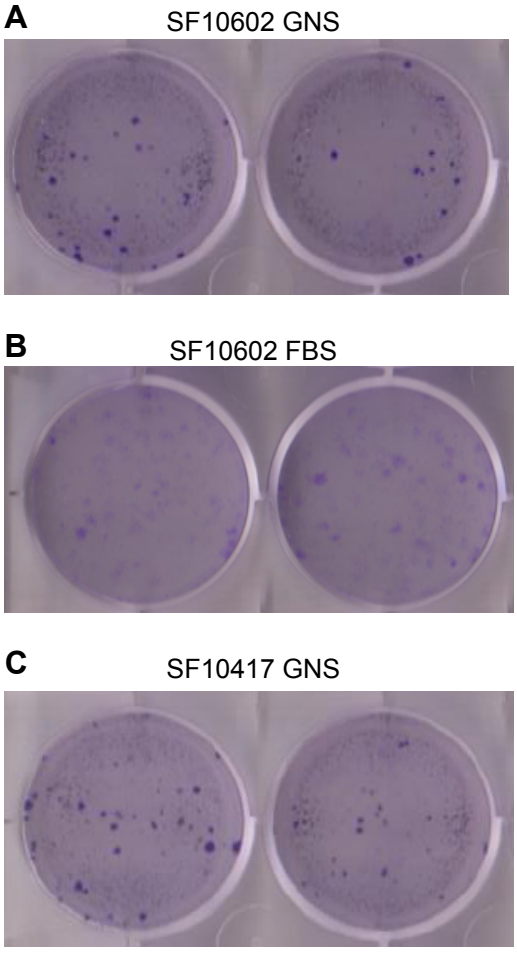

Figure 2.5. HM cell lines demonstrate anchorage-independent growth.
1000 cells each of (**a**), SF10602 GNS, (**b**), SF10602 FBS, and (**c**), SF10417 GNS were seeded into soft agar and stained with crystal violet after four weeks, and yielded an average of 185, 117, and 218 colonies, respectively.

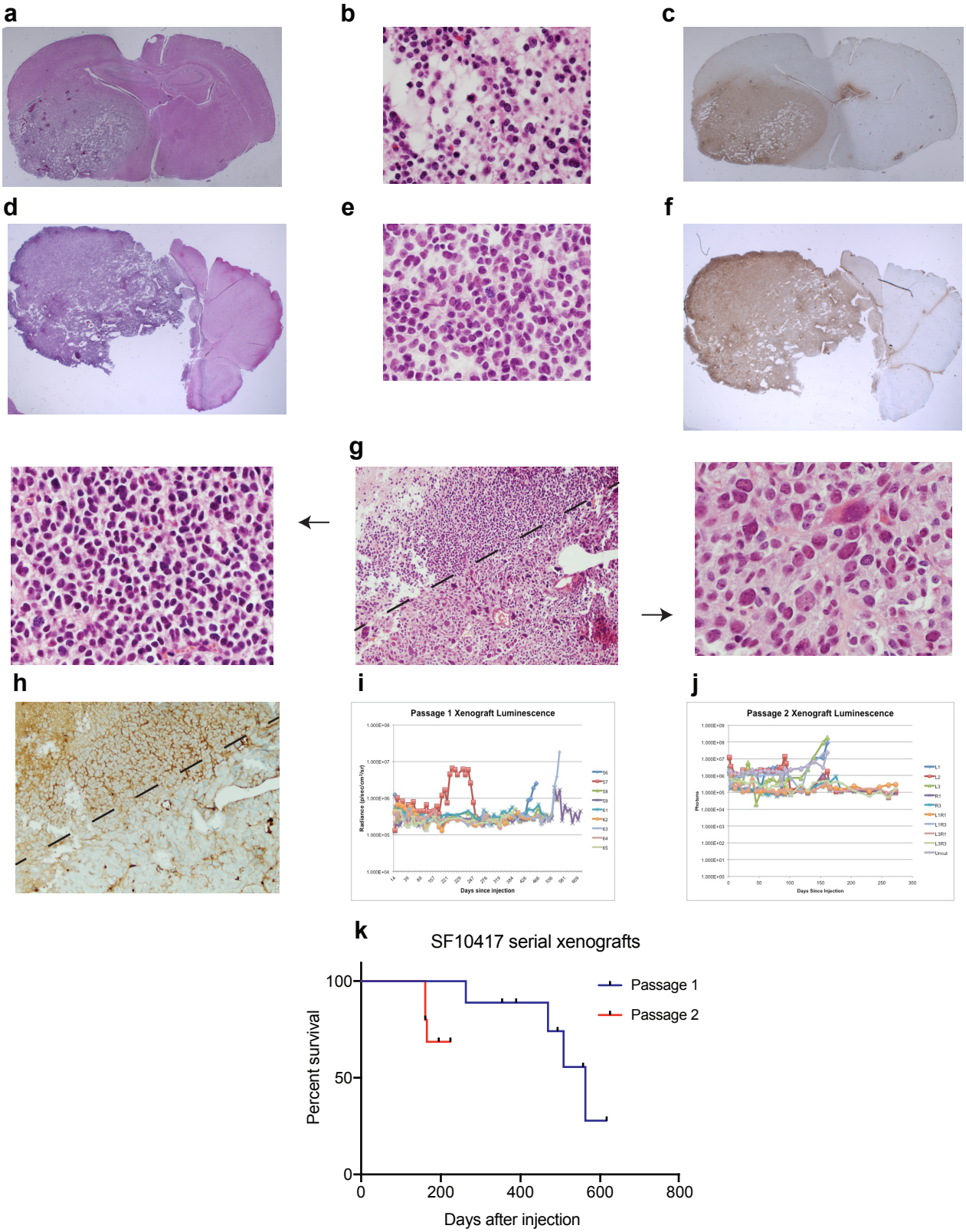

Figure 2.6. SF10417 GNS establishes infiltrative, *IDH1*-mutant intracranial tumors with histologic features characteristic of oligodendroglioma in nude mice.

300,000 cells were implanted into the right cerebrum of five-week old female nude mice. (**a**), H&E staining of a coronal section of mouse brain demonstrating the infiltrative nature of the tumor (1.25X magnification). (**b**), the tumor recapitulates oligodendroglioma histologic features (400X magnification), and (**c**), is positive for IDH1 R132H, by IHC (1.25X magnification). A cell line was established from this tumor and re-implanted in five-week old female nude mice, where (**d**), it again formed infiltrative tumors (1.25X magnification), that (**e**), recapitulate oligodendroglioma histology (400X magnification), and (**f**), are positive for IDH1 R132H by IHC (1.25X magnification). (**g**), one of three serial xenografts tested demonstrated a change in histologic appearance in one part of the tumor (center panel, 100X magnification), from oligodendroglioma-like (left panel, 400X magnification) to prominent anaplastic features with marked nuclear pleomorphism, macronuclei, and high numbers of mitotic figures (right panel, 400X magnification), which (**h**), was accompanied by loss of IDH1 R132H staining (100X magnification). Both (**i**), passage 1 and, (**j**), passage 2 xenografts formed luminescent tumors. (**k**), upon first xenotransplantation, SF10417 GNS formed tumors in four of nine mice over a protracted time period, consistent with the generally slower growth of this tumor subtype. Upon serial xenotransplantation, SF10417 GNS formed tumors in three of nine mice in a reduced time period.

CHAPTER 3: MATERIALS AND METHODS

3.1 SAMPLE ACQUISITION

Fresh surgical specimens were acquired from patients undergoing surgical resection for recurrent glioma after temozolomide treatment by the Neurological Surgery Brain Tumor Center at the University of California, San Francisco (UCSF). Research was approved by the Institutional Review Board at UCSF and sample use was approved by the Committee on Human Research at UCSF. Informed consent was obtained from all patients, and procedures performed in this study are in accordance with the 1964 Helsinki declaration and its later amendments.

3.2 DERIVATION OF PATIENT-DERIVED CELL LINES

Tumor tissue was dissociated with papain (Worthington) for 30 minutes. The suspension was passed through a 70 μM cell strainer, twice, then a 40 μM cell strainer, twice, to achieve a single-cell suspension. Single cells were placed into two media conditions: 1) serum-free, glioma neural stem cell (GNS) medium (*107, 127, 128*), supplemented with EGF (animal-free, Peprotech), bFGF (animal-free, Peprotech) and PDGF-AA (animal-free, Peprotech), or 2) 10% FBS (FBS). GNS media comprised of Neurocult NS-A (Stem Cell Technologies) supplemented with N2 (Invitrogen), B27 (without vitamin A, Invitrogen), 100 μg/mL streptomycin and 100 units/mL penicillin “G” (UCSF Cell Culture Facility), 2 mM L-glutamine (UCSF Cell Culture Facility), and 0.1 mg/mL sodium pyruvate (UCSF Cell Culture Facility). 10% FBS media comprised of DMEM/Ham’s F-12 1:1 Mix (UCSF Cell Culture Facility) supplemented with 10% FBS (Hyclone, characterized), and 100 μg/mL streptomycin and 100 units/mL penicillin “G.” PDLs were grown in a humidified environment at 37 °C with 5% CO_2. The passage of the PDL used is denoted in each experiment. PDLs were determined to be mycoplasma free by testing with the MycoAlert PLUS kit (Lonza).

3.3 SINGLE CELL CLONING

Clones of SF10602 GNS and SF10417 GNS were derived by sparsely seeding 500 cells into laminin-coated 15 cm tissue culture dishes. Colonies formed from single cells were isolated with cloning cylinders and Accutase (Innovative Cell Technologies). 20 clones were derived from SF10602 GNS and 31 from SF10417 GNS. Five SF10602 GNS and four SF10417 GNS clones with different growth rates were selected for exome sequencing.

3.4 DNA ISOLATION

Cells were detached from culture flasks with Accutase, pelleted, and washed with phosphate-buffered saline before pelleting and snap-freezing. DNA was extracted and cleaned from thawed cell pellets and snap-frozen tissue with phenol, chloroform, and isoamyl alcohol as previously described (*89*). DNA was resuspended in TE (Teknova) and stored at 4 °C.

3.5 EXOME SEQUENCING AND MUTATION CALLING

Whole exome capture was performed with SeqCap EZ Exome V3 (Nimblegen) and sequenced on HiSeq 2500 instrumentation (Illumina). Genomic alignment was performed and mutations were called against normal samples as previously described (*89*).

3.6 CONSTRUCTION OF TUMOR PHYLOGENIES

Tumor phylogenies were constructed using ordinary least-squares minimum evolution from a distance matrix of Manhattan distances, as previously described (*129*).

3.7 MUTATIONAL SIGNATURE ANALYSIS

Missense mutations called from whole exome sequencing for each sample were used as input for the mutational signature-calling tool, deconstructSigs (*130*). Resulting mutational signatures, as defined by Alexandrov et al.,(*121*) were quantified by their proportional contribution.

3.8 *IDH1* SANGER SEQUENCING

IDH1 status was validated by PCR with a 2X Phusion High-Fidelity master mix (New England Biolabs, NEB) and Sanger sequencing (Quintara Biosciences), as previously described (*89*). PCR sequences were aligned to a reference sequence using Sequencher (Gene Codes).

3.9 *TERT* PROMOTER SANGER SEQUENCING

TERT promoter (*TERT*p) mutational status was tested as previously described (*131*). Part of the *TERT*p encompassing the common mutations 124 and 146 base pairs upstream of the transcription start site was amplified by PCR with a GC Rich PCR System (Roche) and Sanger sequenced. PCR sequences were aligned to a reference sequence using Sequencher.

3.10 MEASUREMENT OF 2-HG

Metabolites were extracted from 1.5-2.5x10^7 cells using the dual-phase extraction method, magnetic resonance spectra (MRS) acquired, and spectral processing done as previously described (*94*).

3.11 COLONY FORMATION ASSAYS

Growth in soft agar is a well-established phenotype of transformed cells (*132*). 1000 cells were seeded into 0.35% (w/v) ultra-low melting point agarose (Invitrogen) in GNS or FBS media between layers of 0.7% ultra-low melting point agarose in 6-well plates (*93*). After 4-5 weeks, colonies were stained with 0.005% crystal violet (Sigma) and counted under a microscope.

3.12 C-CIRCLE ASSAY

A C-circle assay was performed as previously described (*133*) on DNA that were stored in TE at 4 °C. Briefly, DNA was digested with *Rsa*I and *Hinf*I (NEB) and amplified with Φ29

DNA polymerase. DNA was dotted onto a nylon membrane, crosslinked, and labeled with ^{32}P-$(CCCTAA)_3$.

3.13 TELOMERE RESTRICTION FRAGMENT LENGTH ANALYSIS

Telomere restriction fragment length analysis was done was previously described (*134*). Purified genomic DNA, isolated with phenol/chloroform/isoamyl alcohol (SF10602 GNS, SF10602 FBS, SF10417 GNS) or a DNeasy Blood and Tissue kit (Qiagen, UMUC3 and U2OS) was digested with *Hinf*I, *Alu*I, *Hae*III, *Rsa*I, *Hha*I, and *Msp*I (NEB) and then resolved on an agarose gel. The gel was denatured, dried, and prehybridized. Telomeres were visualized on a Phosphorimager screen after hybridization to a ^{32}P-$(CCCTAA)_3$ probe.

3.14 LUCIFERASE INTRODUCTION

SF10417 GNS and SF10602 GNS were modified to stably express luciferase for use in *in vivo* bioluminescent imaging by infection with Firefly Luciferase Lentifect Purified Lentiviral Particles (Genecopoeia) at an MOI of 7. Cells were exposed to 150 µg/mL luciferin (D-luciferin, Gold Biotechnology) and imaged on an IVIS Spectrum (Perkin Elmer) to confirm stable expression.

3.15 INTRACRANIAL XENOGRAFTS

Animal experiments were performed to comply with current laws of the country and the University of California, San Francisco Institutional Animal Care and Use Committee approved all animal protocols (IACUC protocol AN111064-03B to Dr. Theodore Nicolaides, and IACUC protocol AN175997-01 to Dr. Tomoko Ozawa at UCSF). All animals were housed under aseptic conditions and had access to food and water *ad libidum*.

Primary xenografts were established in five-week old female athymic mice (Simonsen). Mice were anesthetized with 100 mg/kg ketamine and 10 mg/kg xylazine, an incision made in the scalp, and a hole made in the skull with a 25G needle, through which 300,000 luciferase-

modified cells were injected into the caudate putamen, as previously described (*109, 135*). Serial xenografts were established in five-week old female athymic mice (Harlan). Mice were anesthetized with 2-3% isofluorane, an incision made in the scalp, and a hole made with a burr drill through which 300,000 cells were delivered stereotactically to 1.5 mm anterior and 1.5 mm lateral of bregma, and 2.5 mm deep.

Mice were monitored daily until they reached a moribund state or demonstrated 15% weight loss, at which point they were euthanized with CO_2 inhalation followed by cervical dislocation, and brains were immediately removed.

3.16 *IN VIVO* BIOLUMINESCENT IMAGING

Tumor burden was tracked by *in vivo* bioluminescent imaging. After 150 mg/kg luciferin was injected intraperitoneally, mice were anesthetized using 2-3% isofluroane and bioluminescence was recorded after 10 minutes on the IVIS Spectrum (Perkin Elmer). LivingImage software was used to draw regions of interest around the cranium and to record the luminescent reading in photons/s/sr/cm^2 (*109*).

3.17 TISSUE PROCESSING AND ANALYSIS

After removal from euthanized animals, brains were divided into pieces and 1) placed into GNS media for dissociation into culture, 2) flash-frozen for DNA isolation, and/or 3) fixed overnight in 10% neutral buffered formalin. Fixed tissue was embedded in paraffin and sectioned according to routine pathology procedures.

H&E staining was performed, and IHC was performed using a VENTANA BenchMark XT (Roche) or VENTANA Discovery Ultra by the UCSF Brain Tumor Center Tissue Core. Briefly, on the BenchMark, antigen retrieval was performed at 95 °C for one hour, the sample was incubated with a 1:100 dilution of an anti-IDH1 R132H mouse monocolonal antibody (Histobiotec DIANOVA DIA-H09) for one hour at room temperature, detected with the ultraView Universal HRP DAB detection kit (Roche), and stained with hemotoxylin and bluing for twelve

and four minutes, respectively. On the Discovery Ultra, antigen retrieval was performed at 95 °C for 56 minutes, the sample was incubated with a 1:100 dilution of an anti-IDH1 R132H mouse monocolonal antibody (Histobiotec DIANOVA DIA-H09) for one hour at room temperature, detected with the Discovery ChromoMap-DAB kit (Roche), and stained with hemotoxylin and bluing each for four minutes.

CHAPTER 4: DISCUSSION

4.1 CONTRIBUTIONS TO THE FIELD OF NEURO-ONCOLOGY

The successful establishment and characterization of these three *IDH1*-mutant, HM PDLs that retain their key driver mutations and diagnostic molecular features is a novel resource to the neuro-oncology community. These cell lines provide opportunities to study mutant *IDH1*-related epigenomic changes and tumor metabolism, telomerase- and ALT-mediated mechanisms of telomere maintenance and cellular immortality, subclonal dynamics, ITH, mechanisms and consequences of hypermutation, and *in vivo* evolution. These PDLs, or their DNA, RNA, and protein samples, have already been shared for studies with eighteen laboratories across seven institutions (Table 4.1). They have proven instrumental as models of patient-derived, *IDH1*-mutant glioma by contributing to novel discoveries in three published manuscripts and a fourth manuscript recently accepted for publication that enhance our understanding of the regulation of replicative immortality in GBM (*126*), how oligodendroglioma interacts with its microenvironment (*124*), that IDH mutation is important for driving ALT in glioma, and that an IDH mutation-associated upregulation of DNA damage response makes astrocytomas resistant to radiotherapy (Table 4.2).

Additionally, the orthotopic xenografts formed in nude mice formed by SF10417 GNS faithfully recapitulate the histological features of human glioma. Their long and variable time-to-endpoint, while experimentally challenging, is analogous to time-to-recurrence in LGG patients after surgical resection and/or chemoradiotherapy. Another practical asset is that SF10417 GNS can reproducibly passage from *in vitro* to *in vivo* and back. Our sharing of our characterization and cell lines before our own publication speaks to our desire to expand the value of our contribution by enhancing the scientific discoveries of other groups and institutions. Rigorous characterization and open sharing of resources in the neuro-oncology community benefits scientists, clinicians, and most importantly, patients.

4.2 FUTURE DIRECTIONS

4.2.i Xenograft studies

Upon serial xenograft, the time-to-endpoint of SF10417 xenografts was reduced dramatically, although the penetrance did not increase. Exome sequencing on passage two xenografts and their derivative cell lines could be used to elucidate mutated genes or pathways that are enriched during *in vivo* selection and recurrence. Subsequent rounds of *in vivo* passaging may continue to yield a time-to-endpoint that is more experimentally tractable, as seen in our latest results.

4.2.ii Allelic imbalance of IDH

Interestingly, during a second *in vivo* passage, one tumor formed by SF10417 GNS showed loss of IDH1 staining in part of the tumor, which was accompanied by a change in cellular morphology. We and others have observed this phenomenon previously in patients and xenografts (*96, 136-141*), and it deserves additional study as it may impact patient response to targeted therapies. Additional *in vivo* studies may shine light on the frequency of allelic imbalance of IDH, and may provide a mechanism through which to investigate the impact of IDH inhibitors on the frequency and biological consequences of IDH allelic imbalance.

4.2.iii Development of immunotherapies

Hypermutated tumors are predicted to be candidates for successful treatment with immunotherapies due to their neoantigen load (*142, 143*), but brain tumors have proven recalcitrant to immunotherapy due to low levels of immune cells in brain tumors, T-cell exhaustion (*144*), and the challenge of the blood-brain barrier. Despite these unique challenges, initial studies in GBM have shown promise for oncolytic virus treatment (*145*), the ability of chimeric antigen receptor T-cells (CAR-T) to illicit an immune response in the brain (*146*), and mixed, but hopeful results for vaccination approaches (*147, 148*). Our patient-

derived models of HM glioma can enhance the experimental studies that serve as the foundation for these clinical trials: their faithful retention of key driver mutations can be experimentally used to test efficacy of CAR-Ts; sequencing of their high mutation burden can be used to computationally identify neoantigens; their ability to move between *in vitro* and *in vivo* studies makes it possible for preclinical therapeutics identified in cell cultures to be tested in immunocompetent orthotopic xenografts (*149, 150*).

4.2.iv Drug screening

The PDLs characterized in this work are well adapted to tissue culture conditions. GNS lines require laminin coating, specialized media, and growth factors, but grow adherently and therefore could be grown in multi-well formats. The stability and growth characteristics of these lines make them candidates for use in drug screening panels, which is a promising approach being used by one of the labs who received our PDLs. Drug screening could be used to identify specific chemotherapeutic agents or combination(s) of agents that successfully treat rapidly-growing, aggressive HM tumors. There is currently no standard of care for managing patients with HM glioma, and identifying drug(s) that kill HM glioma cells has the potential to significantly improve patient outcomes. Additionally, drug screens that identify novel compounds with efficacy against cells with IDH mutation, telomerase-mediated telomere maintenance, or ALT-mediated telomere maintenance may have implications for many other tumor types.

4.2.v Characterization of additional patient-derived models of glioma and associated stromal cells

During the course of this study, I derived many additional PDLs from patient tissue (Table 4.3). The majority of cultures attempted were from recurrent tumors, and cultures were successfully established in both GNS and FBS media. Some cultures established were not tumor cells (as determined by Sanger sequencing to determine IDH status); these tumor-

associated stromal cells have been studied by others, and the field could benefit from further samples and studies (*151-157*). Additional characterization of patient-derived tumor lines could yield additional *in vitro* and *in vivo* models of HM glioma that maintain key driver and diagnostic mutations.

4.3 TABLES

Table 4.1. Laboratories to which cells or their DNA, RNA, or protein have been distributed.

Principal Investigator	Institution	Location
Dr. Rajit Binda	Yale University	New Haven, CT
Dr. Maria Castro	University of Michigan	Ann Arbor, MI
Dr. Robert Jenkins	Mayo Clinic	Rochester, MN
Dr. Khalid Shah	Harvard University	Cambridge, MA
Dr. Hai Yan	Duke University	Durham, NC
Dr. Chun Zhang Yang	National Cancer Institute	Rockville, MD
Dr. Jing Wu	National Cancer Institute	Rockville, MD
Dr. Diane Barber	University of California, San Francisco	San Francisco, CA
Dr. Elizabeth Blackburn	University of California, San Francisco	San Francisco, CA
Dr. Daniel Lim	University of California, San Francisco	San Francisco, CA
Dr. Hideho Okada	University of California, San Francisco	San Francisco, CA
Dr. Michael Oldham	University of California, San Francisco	San Francisco, CA
Dr. Claudia Petrisch	University of California, San Francisco	San Francisco, CA
Dr. Anders Persson	University of California, San Francisco	San Francisco, CA
Dr. Russ Pieper	University of California, San Francisco	San Francisco, CA
Dr. Sabrina Ronen	University of California, San Francisco	San Francisco, CA
Dr. David Rowitch	University of California, San Francisco	San Francisco, CA
Dr. Valerie Weaver	University of California, San Francisco	San Francisco, CA

Authors	Publication Year	Journal	Title	Institutional Affiliation(s)
Mancini & Xavier-Magalhães et al.	2018	*Cancer Cell*	Disruption of the β1L Isoform of GABP Reverses Glioblastoma Replicative Immortality in a TERT Promoter Mutation-Dependent Manner	University of California, San Francisco
Griveau et al.	2018	*Cancer Cell*	A Glial Signature and Wnt7 Signaling Regulate Glioma-Vascular Interactions and Tumor Microenvironment	Harvard University, University of California, San Francisco, and University of Cambridge
Nunez et al.	2018	Accepted at *Science Translational Medicine*	IDH1R132H acts as a tumor suppressor in glioma via epigenetic upregulation of the DNA damage response	University of Michigan
Mukherjee et al.	2018	*Cancer Research*	Mutant IDH1 cooperates with ATRX loss to drive the alternative lengthening of telomere (ALT) phenotype in glioma	University of California, San Francisco

Table 4.2 Publications resulting from the use of the cell lines described in this work.

Table 4.3 Additional primary cell lines derived during the course of this study.

SF #	Tumor/Stromal	Media	Grade at Culture	Primary/Recurrence
SF10071	Tumor	Serum-free	GBM	Recurrence
SF10324	Stromal	10% FBS	O III	Recurrence
SF10276	Stromal	Serum-free	O III	Recurrence
SF10417	Tumor	Serum-free	O III	Recurrence
SF10577	Stromal	10% FBS	GBM	Recurrence
SF10589	Stromal	10% FBS	A III	Recurrence
SF10602	Tumor	Serum-free	GBM	Recurrence
SF10602	Tumor	10% FBS	GBM	Recurrence
SF10942-1	Tumor	Serum-free	GBM	Recurrence
SF10942-1	Stromal	10% FBS	GBM	Recurrence
SF10942-2	Tumor	Serum-free	GBM	Recurrence
SF10942-2	Tumor	10% FBS	GBM	Recurrence
SF10497	Stromal	Serum-free		
SF10947	Stromal	10% FBS	O II	Recurrence
SF10982	Tumor	Serum-free	GBM	Recurrence
SF10982	Stromal	10% FBS	GBM	Recurrence
Autopsy-S1	Stromal	10% FBS		Recurrence
Autopsy-S2	Stromal	10% FBS		Recurrence
Autopsy-S3	Stromal	10% FBS		Recurrence
Autopsy-S4	Stromal	10% FBS		Recurrence
SF11069	Stromal	10% FBS	O III	
SF11077	Tumor	Serum-free	GBM	Recurrence
SF11253	Stromal	Serum-free	O III	Recurrence
SF11253	Stromal	10% FBS	O III	Recurrence
SF11294-L + AGI-5198	Tumor	Serum-free	GBM	Recurrence
SF11294-L	Stromal	Serum-free	GBM	Recurrence
SF11294-L	Stromal	10% FBS	GBM	Recurrence
SF11294-M + AGI-5198	Tumor	Serum-free	GBM	Recurrence
SF11294-M	Stromal	Serum-free	GBM	Recurrence
SF11294-M	Stromal	10% FBS	GBM	Recurrence
SF11383	Stromal	Serum-free	O II	Primary
SF11468 + AGI-5198	Stromal	Serum-free	A II	Primary
SF11477	Tumor	Serum-free	O II	Recurrent
SF11477	Stromal	10% FBS	O II	Recurrent
SF11479	Stromal	Serum-free	O III	Primary
SF11479 + AGI-5198	Tumor	Serum-free	O III	Primary
SF11506	Stromal	Serum-free		
SF11506	Stromal	10% FBS		

CHAPTER 5: REFERENCES

1. D. N. Louis *et al.*, The 2016 World Health Organization Classification of Tumors of the Central Nervous System: a summary. *Acta Neuropathol* **131**, 803-820 (2016).
2. M. L. Goodenberger, R. B. Jenkins, Genetics of adult glioma. *Cancer Genet* **205**, 613-621 (2012).
3. A. Lai *et al.*, Evidence for sequenced molecular evolution of IDH1 mutant glioblastoma from a distinct cell of origin. *J Clin Oncol* **29**, 4482-4490 (2011).
4. M. Smits, M. J. van den Bent, Imaging Correlates of Adult Glioma Genotypes. *Radiology* **284**, 316-331 (2017).
5. S. Yip *et al.*, Concurrent CIC mutations, IDH mutations, and 1p/19q loss distinguish oligodendrogliomas from other cancers. *J Pathol* **226**, 7-16 (2012).
6. C. Hartmann *et al.*, Type and frequency of IDH1 and IDH2 mutations are related to astrocytic and oligodendroglial differentiation and age: a study of 1,010 diffuse gliomas. *Acta Neuropathol* **118**, 469-474 (2009).
7. N. Cancer Genome Atlas Research *et al.*, Comprehensive, Integrative Genomic Analysis of Diffuse Lower-Grade Gliomas. *N Engl J Med* **372**, 2481-2498 (2015).
8. J. E. Eckel-Passow *et al.*, Glioma Groups Based on 1p/19q, IDH, and TERT Promoter Mutations in Tumors. *N Engl J Med* **372**, 2499-2508 (2015).
9. D. E. Reuss *et al.*, IDH mutant diffuse and anaplastic astrocytomas have similar age at presentation and little difference in survival: a grading problem for WHO. *Acta Neuropathol* **129**, 867-873 (2015).
10. R. B. Jenkins *et al.*, A t(1;19)(q10;p10) mediates the combined deletions of 1p and 19q and predicts a better prognosis of patients with oligodendroglioma. *Cancer Res* **66**, 9852-9861 (2006).
11. C. A. Griffin *et al.*, Identification of der(1;19)(q10;p10) in five oligodendrogliomas suggests mechanism of concurrent 1p and 19q loss. *J Neuropathol Exp Neurol* **65**, 988-994 (2006).

12. C. Bettegowda *et al.*, Mutations in CIC and FUBP1 contribute to human oligodendroglioma. *Science* **333**, 1453-1455 (2011).

13. F. Sahm *et al.*, CIC and FUBP1 mutations in oligodendrogliomas, oligoastrocytomas and astrocytomas. *Acta Neuropathol* **123**, 853-860 (2012).

14. P. J. Killela *et al.*, TERT promoter mutations occur frequently in gliomas and a subset of tumors derived from cells with low rates of self-renewal. *Proc Natl Acad Sci U S A* **110**, 6021-6026 (2013).

15. B. Wiestler *et al.*, ATRX loss refines the classification of anaplastic gliomas and identifies a subgroup of IDH mutant astrocytic tumors with better prognosis. *Acta Neuropathol* **126**, 443-451 (2013).

16. C. M. Heaphy *et al.*, Altered telomeres in tumors with ATRX and DAXX mutations. *Science* **333**, 425 (2011).

17. K. Watanabe *et al.*, Incidence and timing of p53 mutations during astrocytoma progression in patients with multiple biopsies. *Clin Cancer Res* **3**, 523-530 (1997).

18. X. Y. Liu *et al.*, Frequent ATRX mutations and loss of expression in adult diffuse astrocytic tumors carrying IDH1/IDH2 and TP53 mutations. *Acta Neuropathol* **124**, 615-625 (2012).

19. Q. T. Ostrom *et al.*, CBTRUS Statistical Report: Primary brain and other central nervous system tumors diagnosed in the United States in 2010-2014. *Neuro Oncol* **19**, v1-v88 (2017).

20. M. Westphal, K. Lamszus, The neurobiology of gliomas: from cell biology to the development of therapeutic approaches. *Nat Rev Neurosci* **12**, 495-508 (2011).

21. N. Sanai, S. Chang, M. S. Berger, Low-grade gliomas in adults. *J Neurosurg* **115**, 948-965 (2011).

22. H. Bai *et al.*, Integrated genomic characterization of IDH1-mutant glioma malignant progression. *Nat Genet* **48**, 59-66 (2016).

23. M. Ceccarelli *et al.*, Molecular Profiling Reveals Biologically Discrete Subsets and Pathways of Progression in Diffuse Glioma. *Cell* **164**, 550-563 (2016).

24. M. Pekmezci *et al.*, Adult infiltrating gliomas with WHO 2016 integrated diagnosis: additional prognostic roles of ATRX and TERT. *Acta Neuropathol* **133**, 1001-1016 (2017).

25. D. W. Parsons *et al.*, An integrated genomic analysis of human glioblastoma multiforme. *Science* **321**, 1807-1812 (2008).

26. G. P. Dunn *et al.*, Emerging insights into the molecular and cellular basis of glioblastoma. *Genes Dev* **26**, 756-784 (2012).

27. L. Dang *et al.*, Cancer-associated IDH1 mutations produce 2-hydroxyglutarate. *Nature* **465**, 966 (2010).

28. P. S. Ward *et al.*, The common feature of leukemia-associated IDH1 and IDH2 mutations is a neomorphic enzyme activity converting alpha-ketoglutarate to 2-hydroxyglutarate. *Cancer Cell* **17**, 225-234 (2010).

29. W. Xu *et al.*, Oncometabolite 2-hydroxyglutarate is a competitive inhibitor of alpha-ketoglutarate-dependent dioxygenases. *Cancer Cell* **19**, 17-30 (2011).

30. M. Tahiliani *et al.*, Conversion of 5-methylcytosine to 5-hydroxymethylcytosine in mammalian DNA by MLL partner TET1. *Science* **324**, 930-935 (2009).

31. M. E. Figueroa *et al.*, Leukemic IDH1 and IDH2 mutations result in a hypermethylation phenotype, disrupt TET2 function, and impair hematopoietic differentiation. *Cancer Cell* **18**, 553-567 (2010).

32. H. Noushmehr *et al.*, Identification of a CpG island methylator phenotype that defines a distinct subgroup of glioma. *Cancer Cell* **17**, 510-522 (2010).

33. S. Turcan *et al.*, IDH1 mutation is sufficient to establish the glioma hypermethylator phenotype. *Nature* **483**, 479-483 (2012).

34. H. Yan *et al.*, IDH1 and IDH2 mutations in gliomas. *N Engl J Med* **360**, 765-773 (2009).

35. M. Sanson *et al.*, Isocitrate dehydrogenase 1 codon 132 mutation is an important prognostic biomarker in gliomas. *J Clin Oncol* **27**, 4150-4154 (2009).

36. M. Weller *et al.*, Molecular predictors of progression-free and overall survival in patients with newly diagnosed glioblastoma: a prospective translational study of the German Glioma Network. *J Clin Oncol* **27**, 5743-5750 (2009).

37. M. J. van den Bent *et al.*, IDH1 and IDH2 mutations are prognostic but not predictive for outcome in anaplastic oligodendroglial tumors: a report of the European Organization for Research and Treatment of Cancer Brain Tumor Group. *Clin Cancer Res* **16**, 1597-1604 (2010).

38. C. Lu *et al.*, IDH mutation impairs histone demethylation and results in a block to cell differentiation. *Nature* **483**, 474-478 (2012).

39. W. A. Flavahan *et al.*, Insulator dysfunction and oncogene activation in IDH mutant gliomas. *Nature* **529**, 110-114 (2016).

40. D. Rohle *et al.*, An inhibitor of mutant IDH1 delays growth and promotes differentiation of glioma cells. *Science* **340**, 626-630 (2013).

41. P. L. Sulkowski *et al.*, 2-Hydroxyglutarate produced by neomorphic IDH mutations suppresses homologous recombination and induces PARP inhibitor sensitivity. *Sci Transl Med* **9**, (2017).

42. P. Wang *et al.*, Oncometabolite D-2-Hydroxyglutarate Inhibits ALKBH DNA Repair Enzymes and Sensitizes IDH Mutant Cells to Alkylating Agents. *Cell Rep* **13**, 2353-2361 (2015).

43. T. Gorlia *et al.*, New clinical, pathological and molecular prognostic models and calculators in patients with locally diagnosed anaplastic oligodendroglioma or oligoastrocytoma. A prognostic factor analysis of European Organisation for Research and Treatment of Cancer Brain Tumour Group Study 26951. *Eur J Cancer* **49**, 3477-3485 (2013).

44. J. S. Smith *et al.*, Role of extent of resection in the long-term outcome of low-grade hemispheric gliomas. *J Clin Oncol* **26**, 1338-1345 (2008).

45. E. G. Shaw *et al.*, Recurrence following neurosurgeon-determined gross-total resection of adult supratentorial low-grade glioma: results of a prospective clinical trial. *J Neurosurg* **109**, 835-841 (2008).

46. T. Kawaguchi *et al.*, Impact of gross total resection in patients with WHO grade III glioma harboring the IDH 1/2 mutation without the 1p/19q co-deletion. *J Neurooncol* **129**, 505-514 (2016).

47. J. Beiko *et al.*, IDH1 mutant malignant astrocytomas are more amenable to surgical resection and have a survival benefit associated with maximal surgical resection. *Neuro Oncol* **16**, 81-91 (2014).

48. H. Duffau *et al.*, Contribution of intraoperative electrical stimulations in surgery of low grade gliomas: a comparative study between two series without (1985-96) and with (1996-2003) functional mapping in the same institution. *J Neurol Neurosurg Psychiatry* **76**, 845-851 (2005).

49. E. B. Claus *et al.*, Survival rates in patients with low-grade glioma after intraoperative magnetic resonance image guidance. *Cancer* **103**, 1227-1233 (2005).

50. P. M. Black *et al.*, Craniotomy for tumor treatment in an intraoperative magnetic resonance imaging unit. *Neurosurgery* **45**, 423-431; discussion 431-423 (1999).

51. W. Stummer *et al.*, Fluorescence-guided surgery with 5-aminolevulinic acid for resection of malignant glioma: a randomised controlled multicentre phase III trial. *Lancet Oncol* **7**, 392-401 (2006).

52. R. Soffietti *et al.*, Guidelines on management of low-grade gliomas: report of an EFNS-EANO Task Force. *Eur J Neurol* **17**, 1124-1133 (2010).

53. E. G. Shaw *et al.*, Randomized trial of radiation therapy plus procarbazine, lomustine, and vincristine chemotherapy for supratentorial adult low-grade glioma: initial results of RTOG 9802. *J Clin Oncol* **30**, 3065-3070 (2012).

54. B. J. Fisher *et al.*, Phase 2 study of temozolomide-based chemoradiation therapy for high-risk low-grade gliomas: preliminary results of Radiation Therapy Oncology Group 0424. *Int J Radiat Oncol Biol Phys* **91**, 497-504 (2015).

55. M. J. van den Bent *et al.*, Adjuvant procarbazine, lomustine, and vincristine chemotherapy in newly diagnosed anaplastic oligodendroglioma: long-term follow-up of EORTC brain tumor group study 26951. *J Clin Oncol* **31**, 344-350 (2013).

56. J. G. Cairncross *et al.*, Benefit from procarbazine, lomustine, and vincristine in oligodendroglial tumors is associated with mutation of IDH. *J Clin Oncol* **32**, 783-790 (2014).

57. R. Stupp *et al.*, Radiotherapy plus concomitant and adjuvant temozolomide for glioblastoma. *N Engl J Med* **352**, 987-996 (2005).

58. M. J. van den Bent *et al.*, Interim results from the CATNON trial (EORTC study 26053-22054) of treatment with concurrent and adjuvant temozolomide for 1p/19q non-co-deleted anaplastic glioma: a phase 3, randomised, open-label intergroup study. *Lancet* **390**, 1645-1653 (2017).

59. S. Chang *et al.*, Phase III randomized study of radiation and temozolomide versus radiation and nitrosourea therapy for anaplastic astrocytoma: results of NRG Oncology RTOG 9813. *Neuro Oncol* **19**, 252-258 (2017).

60. M. J. van den Bent *et al.*, MGMT-STP27 methylation status as predictive marker for response to PCV in anaplastic Oligodendrogliomas and Oligoastrocytomas. A report from EORTC study 26951. *Clin Cancer Res* **19**, 5513-5522 (2013).

61. M. J. van den Bent *et al.*, Long-term efficacy of early versus delayed radiotherapy for low-grade astrocytoma and oligodendroglioma in adults: the EORTC 22845 randomised trial. *Lancet* **366**, 985-990 (2005).

62. E. Shaw *et al.*, Prospective randomized trial of low- versus high-dose radiation therapy in adults with supratentorial low-grade glioma: initial report of a North Central Cancer Treatment Group/Radiation Therapy Oncology Group/Eastern Cooperative Oncology Group study. *J Clin Oncol* **20**, 2267-2276 (2002).

63. A. B. Karim *et al.*, A randomized trial on dose-response in radiation therapy of low-grade cerebral glioma: European Organization for Research and Treatment of Cancer (EORTC) Study 22844. *Int J Radiat Oncol Biol Phys* **36**, 549-556 (1996).

64. A. Loveless, Possible relevance of O-6 alkylation of deoxyguanosine to the mutagenicity and carcinogenicity of nitrosamines and nitrosamides. *Nature* **223**, 206-207 (1969).

65. B. J. Denny, R. T. Wheelhouse, M. F. Stevens, L. L. Tsang, J. A. Slack, NMR and molecular modeling investigation of the mechanism of activation of the antitumor drug temozolomide and its interaction with DNA. *Biochemistry* **33**, 9045-9051 (1994).

66. J. F. Costello, B. W. Futscher, K. Tano, D. M. Graunke, R. O. Pieper, Graded methylation in the promoter and body of the O6-methylguanine DNA methyltransferase (MGMT) gene correlates with MGMT expression in human glioma cells. *J Biol Chem* **269**, 17228-17237 (1994).

67. J. F. Costello, B. W. Futscher, R. A. Kroes, R. O. Pieper, Methylation-related chromatin structure is associated with exclusion of transcription factors from and suppressed expression of the O-6-methylguanine DNA methyltransferase gene in human glioma cell lines. *Mol Cell Biol* **14**, 6515-6521 (1994).

68. M. Esteller *et al.*, Inactivation of the DNA-repair gene MGMT and the clinical response of gliomas to alkylating agents. *N Engl J Med* **343**, 1350-1354 (2000).

69. M. E. Hegi *et al.*, Clinical trial substantiates the predictive value of O-6-methylguanine-DNA methyltransferase promoter methylation in glioblastoma patients treated with temozolomide. *Clin Cancer Res* **10**, 1871-1874 (2004).

70. M. E. Hegi *et al.*, MGMT gene silencing and benefit from temozolomide in glioblastoma. *N Engl J Med* **352**, 997-1003 (2005).

71. W. P. Roos *et al.*, Apoptosis in malignant glioma cells triggered by the temozolomide-induced DNA lesion O6-methylguanine. *Oncogene* **26**, 186-197 (2007).

72. Y. Hirose, M. S. Berger, R. O. Pieper, p53 effects both the duration of G2/M arrest and the fate of temozolomide-treated human glioblastoma cells. *Cancer Res* **61**, 1957-1963 (2001).

73. G. Marra *et al.*, Tolerance of human MSH2+/- lymphoblastoid cells to the methylating agent temozolomide. *Proc Natl Acad Sci U S A* **98**, 7164-7169 (2001).

74. Z. D. Nagel *et al.*, DNA Repair Capacity in Multiple Pathways Predicts Chemoresistance in Glioblastoma Multiforme. *Cancer Res* **77**, 198-206 (2017).

75. Y. Shinsato *et al.*, Reduction of MLH1 and PMS2 confers temozolomide resistance and is associated with recurrence of glioblastoma. *Oncotarget* **4**, 2261-2270 (2013).

76. A. O. von Bueren *et al.*, Mismatch repair deficiency: a temozolomide resistance factor in medulloblastoma cell lines that is uncommon in primary medulloblastoma tumours. *Br J Cancer* **107**, 1399-1408 (2012).

77. M. M. de las Alas, S. Aebi, D. Fink, S. B. Howell, G. Los, Loss of DNA mismatch repair: effects on the rate of mutation to drug resistance. *J Natl Cancer Inst* **89**, 1537-1541 (1997).

78. S. Haraldsdottir *et al.*, Colon and endometrial cancers with mismatch repair deficiency can arise from somatic, rather than germline, mutations. *Gastroenterology* **147**, 1308-1316 e1301 (2014).

79. H. F. van Thuijl *et al.*, Evolution of DNA repair defects during malignant progression of low-grade gliomas after temozolomide treatment. *Acta Neuropathol* **129**, 597-607 (2015).

80. C. Hunter *et al.*, A hypermutation phenotype and somatic MSH6 mutations in recurrent human malignant gliomas after alkylator chemotherapy. *Cancer Res* **66**, 3987-3991 (2006).

81. N. C. Nicolaides, S. J. Littman, P. Modrich, K. W. Kinzler, B. Vogelstein, A naturally occurring hPMS2 mutation can confer a dominant negative mutator phenotype. *Mol Cell Biol* **18**, 1635-1641 (1998).

82. S. T. Bak, D. Sakellariou, J. Pena-Diaz, The dual nature of mismatch repair as antimutator and mutator: for better or for worse. *Front Genet* **5**, 287 (2014).

83. S. A. Roberts, D. A. Gordenin, Hypermutation in human cancer genomes: footprints and mechanisms. *Nat Rev Cancer* **14**, 786-800 (2014).

84. A. Kat *et al.*, An alkylation-tolerant, mutator human cell line is deficient in strand-specific mismatch repair. *Proc Natl Acad Sci U S A* **90**, 6424-6428 (1993).

85. D. P. Cahill *et al.*, Loss of the mismatch repair protein MSH6 in human glioblastomas is associated with tumor progression during temozolomide treatment. *Clin Cancer Res* **13**, 2038-2045 (2007).

86. N. Cancer Genome Atlas Research, Comprehensive genomic characterization defines human glioblastoma genes and core pathways. *Nature* **455**, 1061-1068 (2008).

87. S. Yip *et al.*, MSH6 mutations arise in glioblastomas during temozolomide therapy and mediate temozolomide resistance. *Clin Cancer Res* **15**, 4622-4629 (2009).

88. W. J. Bodell, N. W. Gaikwad, D. Miller, M. S. Berger, Formation of DNA adducts and induction of lacI mutations in Big Blue Rat-2 cells treated with temozolomide: implications for the treatment of low-grade adult and pediatric brain tumors. *Cancer Epidemiol Biomarkers Prev* **12**, 545-551 (2003).

89. B. E. Johnson *et al.*, Mutational analysis reveals the origin and therapy-driven evolution of recurrent glioma. *Science* **343**, 189-193 (2014).

90. H. Suzuki *et al.*, Mutational landscape and clonal architecture in grade II and III gliomas. *Nat Genet* **47**, 458-468 (2015).

91. M. Scheffner, B. A. Werness, J. M. Huibregtse, A. J. Levine, P. M. Howley, The E6 oncoprotein encoded by human papillomavirus types 16 and 18 promotes the degradation of p53. *Cell* **63**, 1129-1136 (1990).

92. N. Dyson, P. M. Howley, K. Munger, E. Harlow, The human papilloma virus-16 E7 oncoprotein is able to bind to the retinoblastoma gene product. *Science* **243**, 934-937 (1989).

93. Y. Sonoda *et al.*, Formation of intracranial tumors by genetically modified human astrocytes defines four pathways critical in the development of human anaplastic astrocytoma. *Cancer Res* **61**, 4956-4960 (2001).

94. J. L. Izquierdo-Garcia *et al.*, Metabolic reprogramming in mutant IDH1 glioma cells. *PLoS One* **10**, e0118781 (2015).

95. S. Ohba *et al.*, Mutant IDH1 Expression Drives TERT Promoter Reactivation as Part of the Cellular Transformation Process. *Cancer Res* **76**, 6680-6689 (2016).

96. T. Mazor *et al.*, Clonal expansion and epigenetic reprogramming following deletion or amplification of mutant IDH1. *Proc Natl Acad Sci U S A* **114**, 10743-10748 (2017).

97. J. R. Leonard, C. D'Sa, B. J. Klocke, K. A. Roth, Neural precursor cell apoptosis and glial tumorigenesis following transplacental ethyl-nitrosourea exposure. *Oncogene* **20**, 8281-8286 (2001).

98. T. Szatmari *et al.*, Detailed characterization of the mouse glioma 261 tumor model for experimental glioblastoma therapy. *Cancer Sci* **97**, 546-553 (2006).

99. J. Weissenberger *et al.*, Development and malignant progression of astrocytomas in GFAP-v-src transgenic mice. *Oncogene* **14**, 2005-2013 (1997).

100. W. A. Weiss *et al.*, Genetic determinants of malignancy in a mouse model for oligodendroglioma. *Cancer Res* **63**, 1589-1595 (2003).

101. M. Sasaki *et al.*, IDH1(R132H) mutation increases murine haematopoietic progenitors and alters epigenetics. *Nature* **488**, 656-659 (2012).

102. B. Philip *et al.*, Mutant IDH1 Promotes Glioma Formation In Vivo. *Cell Rep* **23**, 1553-1564 (2018).

103. A. L. Cohen, S. L. Holmen, H. Colman, IDH1 and IDH2 mutations in gliomas. *Curr Neurol Neurosci Rep* **13**, 345 (2013).

104. D. R. Laks *et al.*, Large-scale assessment of the gliomasphere model system. *Neuro Oncol* **18**, 1367-1378 (2016).

105. S. K. Singh *et al.*, Identification of human brain tumour initiating cells. *Nature* **432**, 396-401 (2004).

106. R. Galli *et al.*, Isolation and characterization of tumorigenic, stem-like neural precursors from human glioblastoma. *Cancer Res* **64**, 7011-7021 (2004).

107. S. M. Pollard *et al.*, Glioma stem cell lines expanded in adherent culture have tumor-specific phenotypes and are suitable for chemical and genetic screens. *Cell Stem Cell* **4**, 568-580 (2009).

108. J. Lee *et al.*, Tumor stem cells derived from glioblastomas cultured in bFGF and EGF more closely mirror the phenotype and genotype of primary tumors than do serum-cultured cell lines. *Cancer Cell* **9**, 391-403 (2006).

109. T. Ozawa, C. D. James, Establishing intracranial brain tumor xenografts with subsequent analysis of tumor growth and response to therapy using bioluminescence imaging. *J Vis Exp*, (2010).

110. A. Borodovsky *et al.*, A model of a patient-derived IDH1 mutant anaplastic astrocytoma with alternative lengthening of telomeres. *J Neurooncol* **121**, 479-487 (2015).

111. H. A. Luchman *et al.*, An in vivo patient-derived model of endogenous IDH1-mutant glioma. *Neuro Oncol* **14**, 184-191 (2012).

112. J. J. Kelly *et al.*, Oligodendroglioma cell lines containing t(1;19)(q10;p10). *Neuro Oncol* **12**, 745-755 (2010).

113. H. Wakimoto *et al.*, Targetable signaling pathway mutations are associated with malignant phenotype in IDH-mutant gliomas. *Clin Cancer Res* **20**, 2898-2909 (2014).

114. H. Hu *et al.*, Mutational Landscape of Secondary Glioblastoma Guides MET-Targeted Trial in Brain Tumor. *Cell*, (2018).

115. B. B. Campbell *et al.*, Comprehensive Analysis of Hypermutation in Human Cancer. *Cell* **171**, 1042-1056 e1010 (2017).

116. H. Kim *et al.*, Whole-genome and multisector exome sequencing of primary and post-treatment glioblastoma reveals patterns of tumor evolution. *Genome Res* **25**, 316-327 (2015).

117. U. Ben-David *et al.*, Patient-derived xenografts undergo mouse-specific tumor evolution. *Nat Genet* **49**, 1567-1575 (2017).

118. U. Ben-David *et al.*, Genetic and transcriptional evolution alters cancer cell line drug response. *Nature* **560**, 325-330 (2018).

119. K. Tateishi *et al.*, Extreme Vulnerability of IDH1 Mutant Cancers to NAD+ Depletion. *Cancer Cell* **28**, 773-784 (2015).

120. M. Spino *et al.*, Cell surface Notch ligand DLL3 is a therapeutic target in isocitrate dehydrogenase mutant glioma. *Clin Cancer Res*, (2018).

121. L. B. Alexandrov *et al.*, Signatures of mutational processes in human cancer. *Nature* **500**, 415-421 (2013).

122. T. Watanabe, S. Nobusawa, P. Kleihues, H. Ohgaki, IDH1 mutations are early events in the development of astrocytomas and oligodendrogliomas. *Am J Pathol* **174**, 1149-1153 (2009).

123. L. Dang *et al.*, Cancer-associated IDH1 mutations produce 2-hydroxyglutarate. *Nature* **462**, 739-744 (2009).

124. A. Griveau *et al.*, A Glial Signature and Wnt7 Signaling Regulate Glioma-Vascular Interactions and Tumor Microenvironment. *Cancer Cell* **33**, 874-889 e877 (2018).

125. J. Mukherjee *et al.*, Mutant IDH1 Cooperates with ATRX Loss to Drive the Alternative Lengthening of Telomere Phenotype in Glioma. *Cancer Res* **78**, 2966-2977 (2018).

126. A. Mancini *et al.*, Disruption of the beta1L Isoform of GABP Reverses Glioblastoma Replicative Immortality in a TERT Promoter Mutation-Dependent Manner. *Cancer Cell* **34**, 513-528 e518 (2018).

127. B. A. Reynolds, S. Weiss, Generation of neurons and astrocytes from isolated cells of the adult mammalian central nervous system. *Science* **255**, 1707-1710 (1992).

128. Y. Sun *et al.*, Long-term tripotent differentiation capacity of human neural stem (NS) cells in adherent culture. *Mol Cell Neurosci* **38**, 245-258 (2008).

129. T. Mazor *et al.*, DNA Methylation and Somatic Mutations Converge on the Cell Cycle and Define Similar Evolutionary Histories in Brain Tumors. *Cancer Cell* **28**, 307-317 (2015).

130. R. Rosenthal, N. McGranahan, J. Herrero, B. S. Taylor, C. Swanton, DeconstructSigs: delineating mutational processes in single tumors distinguishes DNA repair deficiencies and patterns of carcinoma evolution. *Genome Biol* **17**, 31 (2016).

131. R. J. Bell *et al.*, The transcription factor GABP selectively binds and activates the mutant TERT promoter in cancer. *Science* **348**, 1036-1039 (2015).

132. I. Macpherson, L. Montagnier, Agar Suspension Culture for the Selective Assay of Cells Transformed by Polyoma Virus. *Virology* **23**, 291-294 (1964).

133. J. D. Henson *et al.*, DNA C-circles are specific and quantifiable markers of alternative-lengthening-of-telomeres activity. *Nat Biotechnol* **27**, 1181-1185 (2009).

134. B. S. Herbert, J. W. Shay, W. E. Wright, Analysis of telomeres and telomerase. *Curr Protoc Cell Biol* **Chapter 18**, Unit 18 16 (2003).

135. C. Giannini *et al.*, Patient tumor EGFR and PDGFRA gene amplifications retained in an invasive intracranial xenograft model of glioblastoma multiforme. *Neuro Oncol* **7**, 164-176 (2005).

136. S. Pusch *et al.*, Glioma IDH1 mutation patterns off the beaten track. *Neuropathol Appl Neurobiol* **37**, 428-430 (2011).

137. G. Jin *et al.*, Disruption of wild-type IDH1 suppresses D-2-hydroxyglutarate production in IDH1-mutated gliomas. *Cancer Res* **73**, 496-501 (2013).

138. H. A. Luchman, C. Chesnelong, J. G. Cairncross, S. Weiss, Spontaneous loss of heterozygosity leading to homozygous R132H in a patient-derived IDH1 mutant cell line. *Neuro Oncol* **15**, 979-980 (2013).

139. F. Favero *et al.*, Glioblastoma adaptation traced through decline of an IDH1 clonal driver and macro-evolution of a double-minute chromosome. *Ann Oncol* **26**, 880-887 (2015).

140. C. Chesnelong *et al.*, Lactate dehydrogenase A silencing in IDH mutant gliomas. *Neuro Oncol* **16**, 686-695 (2014).

141. A. Borodovsky *et al.*, 5-azacytidine reduces methylation, promotes differentiation and induces tumor regression in a patient-derived IDH1 mutant glioma xenograft. *Oncotarget* **4**, 1737-1747 (2013).

142. M. S. Rooney, S. A. Shukla, C. J. Wu, G. Getz, N. Hacohen, Molecular and genetic properties of tumors associated with local immune cytolytic activity. *Cell* **160**, 48-61 (2015).

143. T. N. Schumacher, R. D. Schreiber, Neoantigens in cancer immunotherapy. *Science* **348**, 69-74 (2015).

144. K. Woroniecka *et al.*, T-Cell Exhaustion Signatures Vary with Tumor Type and Are Severe in Glioblastoma. *Clin Cancer Res* **24**, 4175-4186 (2018).

145. F. F. Lang *et al.*, Phase I Study of DNX-2401 (Delta-24-RGD) Oncolytic Adenovirus: Replication and Immunotherapeutic Effects in Recurrent Malignant Glioma. *J Clin Oncol* **36**, 1419-1427 (2018).

146. D. M. O'Rourke *et al.*, A single dose of peripherally infused EGFRvIII-directed CAR T cells mediates antigen loss and induces adaptive resistance in patients with recurrent glioblastoma. *Sci Transl Med* **9**, (2017).

147. M. Weller *et al.*, Rindopepimut with temozolomide for patients with newly diagnosed, EGFRvIII-expressing glioblastoma (ACT IV): a randomised, double-blind, international phase 3 trial. *Lancet Oncol* **18**, 1373-1385 (2017).

148. K. A. Batich *et al.*, Long-term Survival in Glioblastoma with Cytomegalovirus pp65-Targeted Vaccination. *Clin Cancer Res* **23**, 1898-1909 (2017).

149. S. Semenkow *et al.*, An immunocompetent mouse model of human glioblastoma. *Oncotarget* **8**, 61072-61082 (2017).

150. C. Garcia *et al.*, The orthotopic xenotransplant of human glioblastoma successfully recapitulates glioblastoma-microenvironment interactions in a non-immunosuppressed mouse model. *BMC Cancer* **14**, 923 (2014).

151. A. Svensson, T. Ramos-Moreno, S. Eberstal, S. Scheding, J. Bengzon, Identification of two distinct mesenchymal stromal cell populations in human malignant glioma. *J Neurooncol* **131**, 245-254 (2017).

152. Q. Zhang *et al.*, CD90 determined two subpopulations of glioma-associated mesenchymal stem cells with different roles in tumour progression. *Cell Death Dis* **9**, 1101 (2018).

153. T. Shahar *et al.*, Percentage of mesenchymal stem cells in high-grade glioma tumor samples correlates with patient survival. *Neuro Oncol* **19**, 660-668 (2017).

154. A. Hossain *et al.*, Mesenchymal Stem Cells Isolated From Human Gliomas Increase Proliferation and Maintain Stemness of Glioma Stem Cells Through the IL-6/gp130/STAT3 Pathway. *Stem Cells* **33**, 2400-2415 (2015).

155. J. Figueroa *et al.*, Exosomes from Glioma-Associated Mesenchymal Stem Cells Increase the Tumorigenicity of Glioma Stem-like Cells via Transfer of miR-1587. *Cancer Res* **77**, 5808-5819 (2017).

156. A. Clavreul *et al.*, Identification of two glioblastoma-associated stromal cell subtypes with different carcinogenic properties in histologically normal surgical margins. *J Neurooncol* **122**, 1-10 (2015).

157. J. Behnan *et al.*, Recruited brain tumor-derived mesenchymal stem cells contribute to brain tumor progression. *Stem Cells* **32**, 1110-1123 (2014).

Publishing Agreement

It is the policy of the University to encourage the distribution of all theses, dissertations, and manuscripts. Copies of all UCSF theses, dissertations, and manuscripts will be routed to the library via the Graduate Division. The library will make all theses, dissertations, and manuscripts accessible to the public and will preserve these to the best of their abilities, in perpetuity.

Please sign the following statement:

I hereby grant permission to the Graduate Division of the University of California, San Francisco to release copies of my thesis, dissertation, or manuscript to the Campus Library to provide access and preservation, in whole or in part, in perpetuity.

Lindsey E Jones
Author Signature

12/9/18
Date